ABSTRACT

AARON ANTHONY CUSHER. Ideal Lift Distributions and Flap Settings for Adaptive Tailless Aircraft. (Under the direction of Dr. Ashok Gopalarathnam.)

With ever increasing maturity in the field of subsonic aircraft design, there exists the desire to tailor the performance of an aircraft to suit specific flight conditions. This has led to several adaptive-wing approaches which seek to improve aircraft performance by changing the wing shape in flight, resulting in drag reduction. One such adaptive-wing approach that has gained considerable popularity is the use of multiple spanwise trailing-edge flaps which are used to optimally distribute the lift of the wing such that drag is minimized. Recent research has been conducted utilizing such a technique applied to an aircraft with a wing-tail configuration and discussed the need to extend these methods to tailless, or all-wing, aircraft, thereby improving design possibilities to include unconventional configurations. The current work explores tailless aircraft configurations which utilize multiple trailing-edge flaps for the purpose of wing adaptation and drag reduction.

As with all tailless aircraft design, the trailing-edge flap settings, and thus wing lift distribution, must be solved while satisfying a longitudinal-pitching-moment constraint in order to ensure longitudinal stability and trim. This is due to the lack of a secondary horizontal surface, such as a tail or canard, which is typically used for stability and trim purposes. The current work implements a numerical approach which was developed to solve for the optimal flap scheduling of a wing with multiple trailing-edge flaps for various flight conditions. Theory presented by R.T. Jones was used as a starting point to solve for the target lift distribution resulting in minimized induced drag with a pitching moment constraint. Also utilized were the ideas of basic and additional lift, as well as thin airfoil theory relations in order to reduce both induced and profile drag by the redistribution of wing lift along its span. The cases were solved with longitudinal trim and lift constraints. The results were presented for planar, tapered wings with multiple quarter-chord sweep angles as well as multiple airfoil sections in order to verify the theory and gain insight into design capabilities and trends. It has been shown

by these results that such adaptive wing methods are applicable and beneficial to tailless aircraft configurations, as reductions in both induced and profile drag have been achieved. In addition, the method is successful for achieving longitudinal trim, and was explored successfully for multiple static margins in order to test the consequence of different longitudinal stability considerations.

Ideal Lift Distributions and Flap Settings for Adaptive Tailless Aircraft

by

Aaron A. Cusher

A thesis submitted to the Graduate Faculty of
North Carolina State University
in partial fulfillment of the
requirements for the Degree of
Master of Science

Aerospace Engineering

Raleigh, NC
2005

APPROVED BY:

Dr. Ashok Gopalarathnam
Advisory Committee Chairman

Dr. Robert T. Nagel
Advisory Committee Member

Dr. Larry M. Silverberg
Advisory Committee Member

BIOGRAPHY

Aaron Anthony Cusher was born to George and Carolyn Cusher April 16th, 1980 in Fargo, North Dakota. The second of three children, Aaron spent his first five years on a small farm operated by his family located in the South Eastern portion of North Dakota. In 1986, Aaron and his family moved off the farm to the big city of Fargo, where he resided through his graduation from Fargo South High School in the Spring of 1998. That fall Aaron moved to Sioux Falls, SD, to attend Augustana College and pursue academic and athletic opportunities. Four years later he graduated cum laude from Augustana with Bachelor of Arts degrees in Mathematics and Computer Science. Immediately following graduation, Aaron accepted a position as a software engineer and analyst at Citibank in Sioux Falls, working in the fast paced world of credit card disputes. Over the next 15 months this corporate environment inspired him to return to school and focus his mathematical abilities on a more applied field. Aerospace Engineering was selected due to past exposure to the subject through an undergraduate research opportunity. In the Fall of 2003 Aaron moved out of the upper Midwest to Raleigh, NC, and enrolled as a Master's student in Aerospace Engineering at North Carolina State University. He joined the applied aerodynamics group at NC State in the Spring of 2004 under the advisement of Dr. Ashok Gopalarathnam, who supported his Master's work.

After completion of his Master's degree Aaron plans to remain at NC State to pursue a doctoral degree in Aerospace Engineering focusing on aeroacoustics under the co-advisement of Dr. Robert Nagel and Dr. Ashok Gopalarathnam.

ACKNOWLEDGEMENTS

I would like to take the time to acknowledge Dr. Ashok Gopalarathnam for his guidance thus far in my graduate studies. I am not sure what possessed him to take a chance on a graduate student with no Aerospace Engineering background, but he did, and I'm grateful. Over the past few years his guidance has inspired my understanding and challenged my abilities.

I would also like to thank Dr. Robert Nagel and Dr. Larry Silverberg for serving on my advisory committee. Moreover, I'd like to thank both of these professors for their interaction with me as I begun my graduate career. My first semester at NC State I was fortunate enough to be a teaching assistant to Dr. Silverberg and take a class from Dr. Nagel. Along with Dr. G, these professors provided my first impressions of Aerospace Engineering at NC State, and their simple acts of friendly conversation provided much needed encouragement, whether they know it or not.

I need to say thank you my parents, George and Carolyn, for all their love, support, and encouragement throughout this process. There is absolutely no doubt in my mind that I wouldn't be here without them and all the sacrifices they have made for me. Both possess the qualities that I strive for in life, and pray to one day achieve. To my brother and sister, Brent and Crysten, I would also like to extend my gratitude. Brent has been a source of academic inspiration my entire life, and through his continued drive for academic success he has, perhaps unknowingly, focused my determination for higher education. And through her honest and free spirited nature, Crysten has inspired me spiritually and personally, always reminding me what is most important in life. I love you all so much.

Table of Contents

List of Tables

List of Figures

Nomenclature

A_0, A_1 coefficients of Fourier series

A, B, C, D constants used in defining normalwash distribution

ac aerodynamic center

AR wing aspect ratio

b wingspan

$\bar{c}$ mean aerodynamic chord

C_D aircraft drag coefficient

C_d airfoil drag coefficient

cg center of gravity

C_L aircraft lift coefficient

C_l airfoil lift coefficient

C_{L_0} aircraft lift coefficient for zero α

C_{la} additional lift coefficient

$C_{la,1}$ additional lift coefficient defined at C_L of one

C_{lb} basic lift coefficient

$C_{lb,camber}$ basic lift coefficient due to airfoil camber

$C_{lb,flap}$ basic lift coefficient due to flap deflection

$C_{lb,twist}$ basic lift coefficient due to wing twist

C_{m_0} zero-lift airfoil pitching moment

$C_{m_{ac}}$ airfoil pitching moment coefficient about the aerodynamic center

$\left(C_{M_{ac_w}}\right)_{basic}$ aircraft pitching moment coefficient about the aerodynamic center resulting from the basic lift distribution

$C_{M,cg}$ aircraft pitching moment coefficient about the center of gravity

$\left(C_{M_{ac_w}}\right)_{sections}$ aircraft pitching moment coefficient about the aerodynamic center resulting from the airfoil sections

C_p airfoil pressure coefficient

$c(y)$ spanwise chord distribution

$\mathbf{I}$ influence coefficient matrix of size $n \times n$

l elemental area of additional lift

LDR low drag range

LHS left hand side

NLF natural laminar flow

N number of flaps per half span of wing

RHS right hand side

S wing area

SM static margin

TAT thin airfoil theory

TE trailing edge

UAV unmanned aerial vehicle

W aircraft weight

w normalwash/downwash in the Trefftz-plane

$\mathbf{w}$ vector containing the n Trefftz-plane normalwash values

X_{ac} longitudinal location of the aerodynamic center

X_{cg} longitudinal location of the center of gravity

Y_{ac} lateral location of the aerodynamic center

α angle of attack

δ_f flap angle

$\bar{\delta}_f$ mean flap angle

$\hat{\delta}_f$ variation flap angle about the mean

Γ bound vorticity strength

γ local circulation as described by TAT

$\mathbf{\Gamma}$ vector of the n bound-vortex strengths

Λ quarter-chord sweep angle

θ_f angular location of flap hinge in radians

Subscripts

$desired$ desired condition

f flap

$ideal$ ideal condition

∞ freestream condition

$wing$ wing

Superscripts

$elliptic$ matches elliptical loading

Chapter 1

Introduction

As part of an on-going research effort on adaptive wing technology, this thesis describes work that was focused on determining ideal flap angles and lift distributions on adaptive wings for longitudinally-stable tailless aircraft that are required to satisfy a given longitudinal trim constraint.

Recent research[1] has been conducted on the use of a multiple trailing-edge (TE) cruise flaps distributed across a wing span with the goal of achieving optimal lift distributions, and thus reduced drag. In that effort, there was no constraint on the longitudinal trim, as it was assumed that the wing was the primary lifting surface on a wing-tail aircraft configuration and that the horizontal tail would be used for trimming the airplane. Modern aircraft usage and design has shown that other configurations have gained popularity, and should be considered viable options for future aircraft design. One such configuration is the tailless aircraft. With the removal of the horizontal tail, however, the direct ability to trim the aircraft is lost, forcing the focus of trim to proper wing design. Thus, in designing an adaptive wing to reduce drag for use on a tailless aircraft, lift distributions must be described that satisfy the trim constraint in addition to achieving low drag, which was the focus of this work.

Presented in Sec. 1.1 is background information pertaining to tailless aircraft and their benefits. Next, Sec. 1.2 describes multiple spanwise trailing-edge flaps,

and the use of adaptive wing technology for the reduction of drag. Lastly, a brief outline of the thesis is provided in Sec. 1.3.

1.1 Tailless Aircraft

Over the past 100 years, although most aircraft have been designed with a wing (as the primary lifting surface) and an aft tail (for stability and trim), there have been several unconventional configurations. Tailless aircraft are examples of unconventional configurations. Throughout this thesis, the term "tailless aircraft" will be used to describe those aircraft that are designed with only one main lifting surface, that being the wing, which is responsible for producing the aircraft's lift and also contains all control surfaces providing static and dynamic stability. These aircraft are sometimes referred to as flying wings, blended-wing bodies, or all-wing aircraft. The more conventional two horizontal element designs, as indicated by the vast majority of commercial aircraft, will be referred to as "tailed aircraft."

However modest, tailless aircraft configurations have found popularity along side tailed configurations in particular applications. These applications include sailplanes and gliders, light airplanes, unmanned aerial vehicles (UAV), high-speed military planes, supersonic airliners, and hypersonic re-entry vehicles.[2] One need not look any further than the Northrup B-2 "stealth"-bomber in order to get a sense of the potential that future tailless designs hold. And because only one lifting surface is used, it has often been proposed that drag benefits should be realized and design costs kept lower when implementing a tailless design verses a comparable tailed design.[3] Despite these positives, tailless configurations have seen limited use in general aviation and commercial aircraft design, most likely due to inherent complexity in the aerodynamic design of tailless aircraft and perhaps also due to the overwhelming history of tailed-aircraft use, giving indication of

the need for the advancement in tailless design technology.

One hindrance to the development of tailless aircraft is the idea that these aircraft present difficulty for achieving longitudinal stability and trim, as pointed out by Kroo.[4] With seemingly limitless parameters used in modern aircraft design, including wing and tail geometry variables, engine size, and operational parameters for several flight conditions, it is understandable that the conservative tailed design has stood the test of time as it satisfies trim with little optimization necessary.[5] However, analysis by Kroo has shown that the removal of an aircraft's tail can result in aircraft gross weight, fuel consumption, and direct operating cost reduction when compared to similar tailed configurations.[5] And further, by employing the design philosophy of Reimar and Walter Horten of Germany that has the lift at the wing tips nearly zero and utilizes twist to push much of the lift inboard, a tailless aircraft that is very stable longitudinally is possible.[3] In fact, this method describes the classic bell-shaped lift distribution that is typical of successful designs employed on modern tailless aircraft.

Although tailless aircraft have found most favor with UAV and military applications, there is evidence that such a configuration may one day be utilized by the commercial airline industry. The Boeing Company, in a joint venture with NASA, has recently been exploring a "blended-wing-body" (BWB) concept that has shown preliminary improvements in airliner efficiency.[3] Boeing studies have shown 15% reduction in sized take-off weight, 20% improvement in L/D, 27% reduction in fuel usage, 27% lower thrust, and 12% lower operating empty weight when compared to a similar tailed design.[6] The design has a large delta-shaped wing/fuselage center section which accommodates a two-story passenger cabin. A conceptual sketch of this vehicle is provided in Fig. 1.1. Such a design leads to reductions in root bending moments stresses, as the fuselage is largely incorporated in the wing section. It seems that this a design most suited for a very

large airliner, however negatives such as a large, windowless cabin may lead to passenger discomfort, and need to be addressed.

Figure 1.1: Blended-wing-body (BWB) airliner concept (courtesy NASA).

The use of adaptive wing technology on tailless aircrafts is not a new concept, as examples exist readily in nature in the form of birds, butterflies, and insects. Many of these animals possess excellent flying characteristics despite the fact that they have little or no tails, and might be viewed as models for man-made tailless aircraft. Further, it has been viewed that although some birds do possess a horizontal tail, the tail has virtually no stabilizing effect and hence is not a stabilizing instrument.[2] This concept is different from that used by tailed aircraft, thus making adaptive tailless aircraft closer to birds then their tailed counterparts. Other examples of tailless aircraft in nature are certain varieties of seeds, notably the Zanonia seed,[2] which grow wings that surround their seed, placing the seed,

and thus the center of gravity, in an optimal location for gliding. These shapes have been implemented on aircraft such as hang-gliders, where the center of gravity shift provides control, leading to the existence of no control surfaces, and directly to an adaptive concept. This thesis will explore similar adaptive tailless aircraft designs, focusing on the use of multiple trailing edge flaps for minimizing drag while achieving longitudinal trim.

1.2 Multiple Trailing-Edge Flaps and Adaptive Wings

Historically, wing design has focused on rigid, inflexible shapes that are tailored to the specific flight conditions for which the airplane is designed. As an example, a typical commercial airliner maintains the same wing configuration throughout the majority of its flight despite changing conditions such as weight reduction due to the burning of fuel. In fact, the primary method, and often solitary method, of wing adaptation employed today is the use of high-lift devices for take-off and landing procedures, which account for a minuscule amount of the flight envelope. If a wing were allowed to adapt to the changing conditions throughout the majority of its flight, efficiency benefits could be assumed. This idea gives rise to the desire for adaptive wings, as benefits of adaptive wings have been shown in numerous numerical and experimental studies.[7–11]

Several methods can be used for creating an adaptive wing. One such method is the utilization of multiple trailing-edge flaps which modify the spanwise camber of the wing, and is the method of wing adaptation that has been used by this study. Figure 1.2 displays a planform view of a multiple TE flap configuration. Through the use of multiple TE flaps it is possible to prescribe the camber at any spanwise location, thus affecting the spanwise lift distribution of the wing. It

is possible, then, to solve for the TE flap settings that result in a desirable lift distribution based on necessary constraints, resulting in reduced drag.

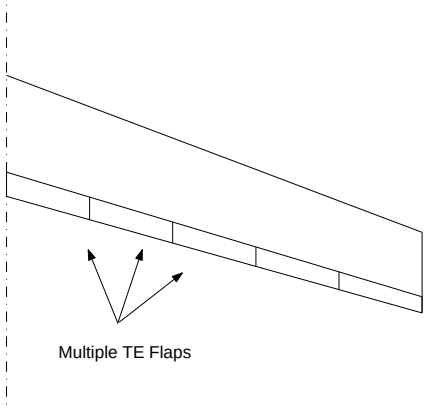

Figure 1.2: Schematic representation of the planform of a wing with multiple trailing-edge flaps (right side shown).

It is well known that for a tailless aircraft the distribution of lift not only accounts for drag characteristics, but also plays a large role in the aircraft's ability to achieve longitudinal trim. This arises from the dependence that the spanwise lift distribution of a aft-swept wing, typical of tailless aircrafts, has on the wing pitching moment. If one considers an aft-swept wing with its aerodynamic center located near half its semispan, as displayed in Fig. 1.3, then positive lift acting forward of $X_{ac,wing}$ will result in a nose-up pitching moment, while positive lift acting aft of $X_{ac,wing}$ results in a nose-down moment. The importance that lift plays for determining wing pitching moment is heightened when considering tailless aircraft, as the lack of a secondary horizontal lifting surface creates reduced opportunity for compensating for wing pitching-moment changes. Despite this shortcoming, successful tailless designs have found favor in many situations. Further, spanwise camber change, similar to that researched in the current work, has

been utilized extensively on tailless hang gliders for years, as the shape of the flexible sail is allowed to change as weight is shifted and trim is achieved. It is not unreasonable to assume that this technology can be extended to other rigid-wing aircraft.

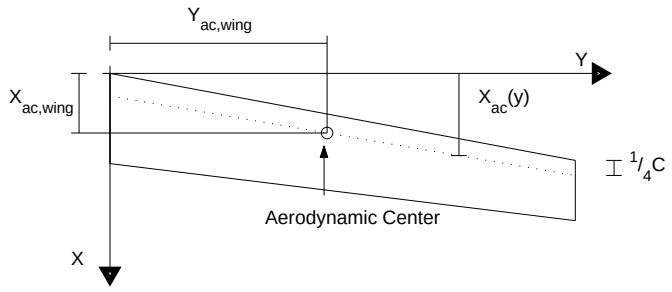

Figure 1.3: Orientation of half-span wing aerodynamic center.

The benefits and increasing interest in multiple trailing-edge flap technology has led to several advances in the area. Recent research conducted at North Carolina State University by King and Gopalarathnam[1] has provided methodology for determining the optimal flap settings of an aircraft which utilizes multiple spanwise TE flaps in order to reduce both induced and profile drag while satisfying an optional root-bending-moment constraint. For that study, the system was solved for an aircraft utilizing a wing-tail configuration, where the tail was used for purposes of achieving longitudinal trim. That research was conducted following successful tests of an auto-adaptive airfoil section by McAvoy and Gopalarathnam,[12,13] in which pressure ports located on the airfoil were used to position a TE "cruise flap" in order to optimally locate the stagnation point at the leading edge and thus reduce profile drag by achieving favorable pressure distributions that support extensive laminar flow over a wide range of lift coefficients. A combination of these past research efforts leads to the direct possibility for an automated adaptive wing. It is the goal of the current research to explore the applicability

of multiple TE flaps to tailless configurations where an additional constraint of longitudinal trim needs to be satisfied.

1.3 Outline of Thesis

This chapter has provided not only the motivation for conducting the research presented here, but has also focused on previous concepts and research pertaining to the current research. Moving forward, chapter 2 describes the background material and procedures utilized in this thesis. First presented is the background information pertaining to the relationship between aircraft pitching moment and static margin. Next are discussions relating to achieving minimum induced and profile drag, as well as the concept of additional and basic lift distributions, which was utilized extensively during this research. This is followed by the methodology used for defining aircraft pitching moment for the current problem, then describes the reduction of both induced and profile drag for adaptive tailless aircraft. Results are presented in chapter 3 and display the concepts of induced-drag reduction and profile-drag reduction on example planar configurations. Chapter 4 will provide a brief conclusion of the research as well as present some suggested future work.

Chapter 2

Methodology

2.1 Background

This section describes background information relevant to determining optimum TE flap angles for adaptive tailless aircraft. The theory presented here has been derived from well-known applied aerodynamics, and is presented in the following subsections. Section 2.1.1 provides a brief introduction to the pitching moment constraint required by this problem and how it relates to static margin. Section 2.1.2 describes the methodology for reducing induced drag of an adaptive tailless aircraft given longitudinal trim and lift constraints. Profile drag is addressed in Sec. 2.1.3, which describes the use of thin airfoil theory relations for determining the C_l-shift in the drag bucket of a NLF airfoil due to TE flap deflection. Lastly, Sec. 2.1.4 describes the theory of basic and additional lift distributions, which was used extensively for solving the problem at hand.

2.1.1 Static Margin and Pitching Moment Constraint

Stated in Sec. 1.2 was the importance that wing pitching moment has for the current problem. This subsection seeks to explain this importance further by introducing the relationships between the moment about the cg, the moment

about the ac, and static margin. Equation 2.1 presents this relationship for an airfoil in coefficient form where $\frac{(X_{ac}-X_{cg})}{\bar{c}}$ is commonly known as the static margin.

$$C_{m_{cg}} = C_{m_{ac_w}} - C_l \frac{(X_{ac} - X_{cg})}{\bar{c}} \tag{2.1}$$

Figure 2.1 provides a graphical presentation of the terms in this equation, where

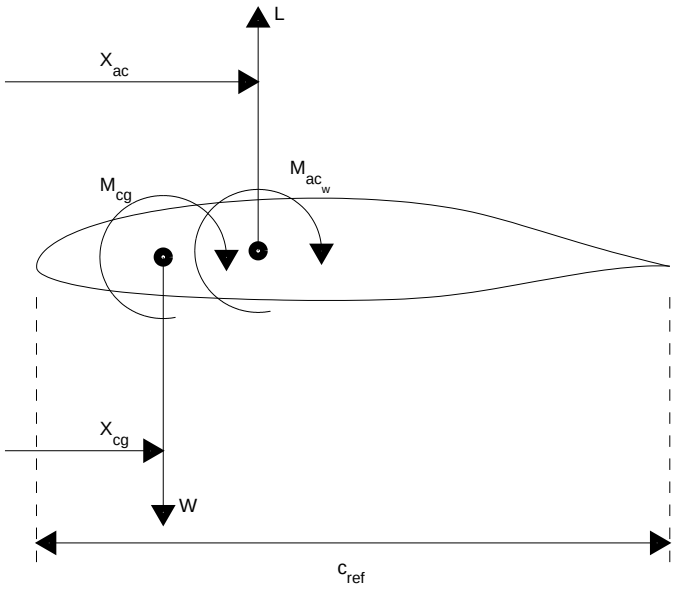

Figure 2.1: Forces applied to an airfoil representing the relationship between pitching moments and SM.

c_{ref} is equivalent to the mean aerodynamic chord $\bar{c}$. It follows that for a given static margin and C_l the necessary condition for longitudinal trim ($C_{m_{cg}} = 0$) can be rewritten in terms of a desired $C_{m_{ac_w}}$, as shown in Eq. 2.2.

$$C_{m_{ac_w}} = C_l \frac{(X_{ac} - X_{cg})}{\bar{c}} \tag{2.2}$$

Thus if a tailless aircraft is required to fly at a desired C_L with a known static margin, the $C_{M_{ac_w}}$ needs to be constrained as per Eq. 2.2. The significance of this

is highlighted in the current work, as upcoming sections will show the value $C_{M_{ac_w}}$ to be the primary constraint for each drag reduction scheme and is a necessity for ensuring successful results.

2.1.2 Minimum Induced Drag with Pitching Moment Constraint

The primary goal of aerodynamicists is often to minimize drag. This has led to numerous achievements over the past century in all areas of drag reduction, including induced drag. Induced drag is labeled as such because it is induced by the downwash of the wing, which causes a tilt of the lift vector, leading to drag. This type of drag is most dominant at high C_L, and has been studied extensively in the past. It is well known that minimum induced drag for a planar wing results from elliptical loading. Therefore, methods to achieve elliptical loading, such as wing twist and camber changes, have been employed in wing design for many years. The current work focuses on reducing induced drag by achieving an optimal lift distribution through the use of multiple TE flaps. This concept is applied to tailless aircraft, forcing the need for solving the optimum lift distribution that also satisfies a pitching moment constraint, due to the fact that longitudinal trim of tailless aircraft is heavily reliant on a properly designed lift distribution.

R.T. Jones has provided the methodology for determining the lift distribution for minimum induced drag with a constraint on the root-bending-moment,[14] which was used as a template for the current work. However, as it is necessary for the design of tailless aircraft, the root-bending moment constraint described by Jones was replaced with the pitching-moment-constraint for the current effort. As stated by Jones, if induced drag is to be minimum then small variations in the shape of the lift distribution, that satisfy the constraints, will not cause first-order changes

in induced drag.[14] Figure 2.2 displays the right hand side of a symmetric loading

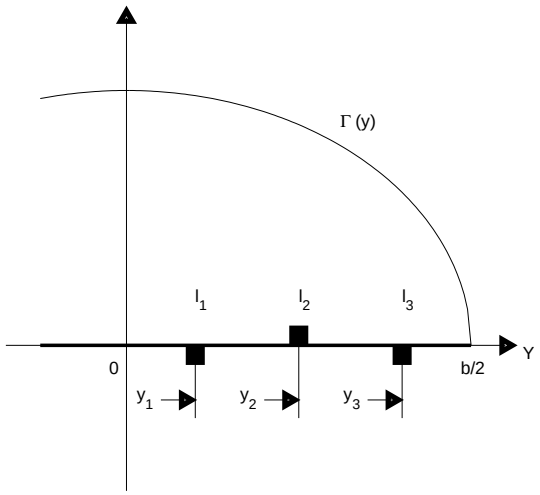

Figure 2.2: Spanwise loading curve of a planar wing with three elements of variation.

that is assumed to result in minimum induced drag while satisfying a constraint on the pitching moment due to loading. The figure also shows three elemental variations in lift which are labeled l_1, l_2, and l_3 at spanwise locations y_1, y_2, and y_3. This distribution is referred to as the original lift distribution and the importance of the variations in lift will be indicated in the upcoming discussion. The location of the spanwise wake trace along the wing is denoted y and exists between wing root location 0 and wing tip location $b/2$. The resulting bound-vorticity distribution, $\Gamma(y)$, can be used to compute the lift of the wing, as shown in Eq. 2.3.

$$L = 2\rho V_\infty \int_0^{\frac{b}{2}} \Gamma(y) dy \tag{2.3}$$

The pitching moment of the wing about its aerodynamic center due to lift can now be determined, and is solved for beginning with Eq. 2.4.

$$M_{ac,wing} = 2\int_0^{\frac{b}{2}} C_{m_{ac}}(y) c(y)^2 q_\infty dy + 2\int_0^{\frac{b}{2}} C_l(y)[X_{ac,wing} - X_{ac}(y)] c(y) q_\infty dy \tag{2.4}$$

The first term in the RHS of Eq. 2.4 is the contribution from the airfoil section moments when integrated across the span, while the second term is the contribution to the moment from the lift distribution acting on an aft-swept quarter-chord line. In this subsection, only the contribution due to lift distribution is considered. The section contribution is discussed later in the chapter. Thus, it follows that the contribution of the lift distribution to the wing pitching moment $M_{ac,wing}$ about the aerodynamic center is computed using the Γ distribution, and is shown in Eq. 2.5.

$$M_{ac,wing} = 2\rho V_\infty \int_0^{\frac{b}{2}} \Gamma(y)[X_{ac,wing} - X_{ac}(y)]dy \tag{2.5}$$

In this equation the value $X_{ac,wing}$ is the longitudinal location of the wing aerodynamic center, while $X_{ac}(y)$ is the location of the aerodynamic center of the airfoil section at spanwise location y, as shown in Fig. 2.3.

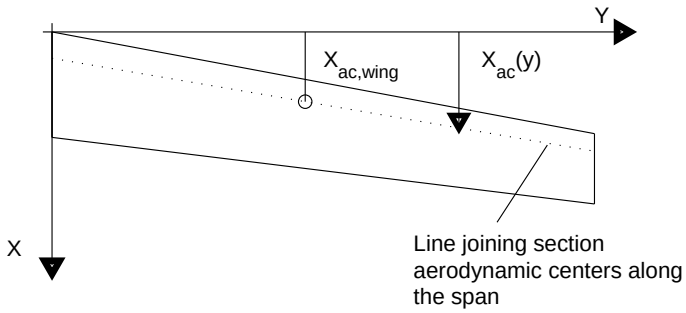

Figure 2.3: Graphical representation of $X_{ac,wing}$ and $X_{ac}(y)$.

Finally, induced drag can be calculated in a manner similar to lift and wing pitching moment, as shown by Jones. For this calculation the Trefftz-plane normalwash distribution ($w(y)$) was used along with the Γ distribution, and is displayed in Eq. 2.6.

$$D_i = \rho \int_0^{\frac{b}{2}} w(y)\Gamma(y)dy \tag{2.6}$$

With the necessary equations and methods in place, it is now desirable to solve for the downwash distribution that results in minimum induced drag with constraints on lift and pitching moment. The procedure of Jones was followed further, and the three variations in the lift were selected as to maintain the desired results; namely, no change in lift (Eq. 2.7), no change in pitching moment (Eq. 2.8), and the maintenance of minimum induced drag (Eq. 2.9). The discrete variation in the loading l_1, l_2, and l_3 as well as their spanwise locations y_1, y_2, and y_3 used in the equations below are as shown in Fig 2.2.

$$\Delta L = 0 : l_1 + l_2 + l_3 = 0 \tag{2.7}$$

$$\Delta M_{cg} = 0 : l_1[X_{ac,wing} - X_{ac}(y_1)] + l_2[X_{ac,wing} - X_{ac}(y_2)] + l_3[X_{ac,wing} - X_{ac}(y_3)] = 0 \tag{2.8}$$

$$\Delta D_i = 0 : l_1 w_1 + l_2 w_2 + l_3 w_3 = 0 \tag{2.9}$$

Because the spanwise locations y_1, y_2, and y_3 were chosen arbitrarily, it can be shown that solving this system of equations for the Trefftz-plane normalwash $w(y)$ results in Eq. 2.10,

$$w(y) = A + B(X_{ac,wing} + (y\tan\Lambda)) \tag{2.10}$$

where Λ represents the quarter-chord sweep angle of the wing and A and B represent arbitrary constants to be solved. Further, because of the nature of the constants this equation can be simplified to

$$w(y) = C + Dy \tag{2.11}$$

where $C = A + BX_{ac,wing}$ and $D = B\tan\Lambda$. The values C and D are determined by specifying the desired lift and pitching moment constraints for the wing of

known planform geometry (known values for $X_{ac,wing}$ and Λ).

The resulting $w(y)$ distribution and the corresponding $\Gamma(y)$ distribution are closely related, and can be determined using a discrete vortex method similar to that described by Blackwell.[15] For the current research, the computer program from the earlier research of King and Gopalarathnam[1] was adapted. This method has the bound vorticity distribution and the trailing vorticity shed behind it approximated using n horseshoe vorticies, each having constant bound vortex strength Γ. This procedure results in the n-dimensional Γ vector being related to the n-dimensional $\mathbf{w}$ vector by a $n \times n$ influence coefficient matrix $\mathbf{I}$, as displayed in Eq. 2.12.

$$\mathbf{I} \cdot \mathbf{\Gamma} = \mathbf{w} \tag{2.12}$$

Thus for a given $w(y)$, the $\Gamma(y)$ can be determined. From the knowledge of $\Gamma(y)$ and $w(y)$, Eqs. 2.3, 2.5, and 2.6 can be used to solve for wing lift, pitching moment, and induced drag. The $C_l(y)$ distribution can also be determined using Eq. 2.13, where $c(y)$ is the spanwise chord distribution and V_∞ is freestream velocity, and will be utilized later in the methodology section.

$$C_l(y) = \frac{2}{c(y)} \frac{\Gamma(y)}{V_\infty} \tag{2.13}$$

In order to determine $\Gamma(y)$, it is required to first solve $w(y)$. This was accomplished, as described previously, by solving for the two constants C and D of Eq. 2.11. This was done by utilizing a single step of Newton's method, with the equation displayed in Eq. 2.14, where the Jacobian of partial derivatives were computed using finite differencing. For example, in order to compute $\frac{\partial L}{\partial C}$, a small change in C was made and the resulting change in L was recorded. The RHS of the equation is simply the desired values of lift and pitching moment. Thus, the

values of C and D can be extracted and the downwash distribution $w(y)$ can be obtained.

$$\begin{pmatrix} \frac{\partial L}{\partial C} & \frac{\partial L}{\partial D} \\ \frac{\partial M_{ac,wing}}{\partial C} & \frac{\partial M_{ac,wing}}{\partial D} \end{pmatrix} \begin{pmatrix} C \\ D \end{pmatrix} = \begin{pmatrix} L \\ M_{ac,wing} \end{pmatrix} \tag{2.14}$$

Figure 2.4 provides a visual representation of some results obtained using the methods described above. In this example, a hypothetical planar wing with ta-

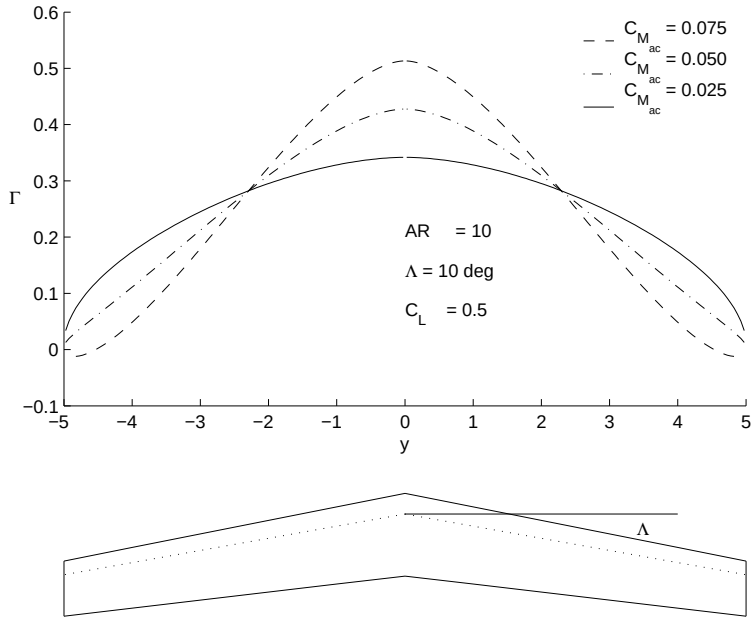

Figure 2.4: $\Gamma(y)$ distribution resulting in minimum induced drag for a family of pitching moment constraints about the aerodynamic center of the geometry displayed.

per ratio of $\frac{2}{3}$ and quarter-chord sweep angle of 10 degrees aft was analyzed for multiple pitching moment constraints. The family of constraints displayed are 0.075, 0.050, and 0.025, while lift coefficient was maintained at 0.5. Recall that the constraints represent the contribution of the lift distribution to the pitching moment coefficient about the aerodynamic center of the wing. The lower portion of Fig. 2.4 displays a visual representation of the wing planform, while the upper portion gives the plots of the spanwise wing loadings. It can be said that these loadings will satisfy the constraints mentioned above while in each case producing

minimal induced drag. From the $\Gamma(y)$ distribution, the C_l distribution can be extracted and matched, ensuring minimized induced drag.

2.1.3 Minimum Profile Drag

The second type of drag that was addressed by the current problem is profile drag. Minimizing profile drag is largely the goal during high-speed cruise conditions (low-C_l), when high efficiency is desired. For the case of low subsonic Mach numbers, profile drag is primarily a result of skin friction. Because of this, considerable effort has been placed on developing airfoils and wings that maintain large sections of favorable pressure gradient on both the upper and lower surfaces in order to support laminar flow. These airfoils are known as Natural Laminar Flow airfoils, and are typically designated NLF. A common characteristic of NLF airfoils is the presence of a low drag range (LDR), or drag bucket, that surrounds the design C_l of that airfoil. This LDR is a result of the stagnation point of the unflapped airfoil residing within an optimal region of the airfoil's leading edge. The angle-of-attack (α) that corresponds to the C_l value, labeled C_{lideal}, in the middle of the LDR is deemed α_{ideal}, and is the design α for minimized profile drag. If the α of the airfoil is such that the stagnation point is located outside the optimal region, very often a steep rise in drag will result, signifying operation outside the LDR. This is most commonly due to a section peak that has formed on either the upper or lower surface of the airfoil, causing the flow to transition from laminar to turbulent resulting in increased skin-friction drag.

Thin airfoil theory (TAT) can be used to calculate the α_{ideal} of an NLF airfoil, and thus the middle of the LDR. By employing TAT relations, if the stagnation point is located at the leading edge of the airfoil, then $\gamma(LE) = 0$, where $\gamma(LE)$ is the value of the circulation at the leading edge, and the result will be no suction peaks. If this condition is met, then it follows that $A_0 = 0$, where A_0 is the first

coefficient in the Fourier series that is typically used to describe the chordwise circulation distribution for the airfoil.[16] Thus, provided a camberline, TAT can be used to solve for the value of α_{ideal}, which correlates to the airfoil's C_{lideal}. An easy example of this concept is $\alpha_{ideal} = 0$ deg for an unflapped, symmetric airfoil.

In several situations, it has been desirable to shift the LDR of an airfoil to higher or lower C_l values in order to increase its low-drag operating capability. To achieve this, the use of trailing-edge "cruise" flaps have been employed. Cruise flaps were first introduced by Pfenninger,[17,18] and are used extensively on high-performance sailplanes,[19] as well as several other applications.[19–25] The concept of the cruise flap is that by deflecting a TE flap, the camber of the airfoil is changed, and results in a corresponding change in C_{lideal}. TAT provides the direct relationship between change in C_{lideal} and flap deflection, which is provided in Eq. 2.15,

$$\Delta C_{lideal} = (\pi A_1)\delta_f = (2\sin\theta_f)\delta_f \tag{2.15}$$

where δ_f represents the flap angle in radians, θ_f is the angular coordinate for the hinge location $\frac{x_f}{c}$ in radians as described by Eq. 2.16, and A_1 is one of the Fourier coefficients used to define the chordwise circulation distribution.

$$\theta_f = \cos^{-1}\left(1 - 2\frac{x_f}{c}\right) \tag{2.16}$$

By making use of the concepts described above, it is possible to predictably shift the LDR of an NLF airfoil to encompass a C_l value, and thus providing minimized profile drag for a greater range of C_l values.

The methods explained above have particular consequences for the current problem, as a flap deflection that reduces profile drag will result in a pitching moment change. Thus, it is necessary to consider this change, which can also be predicted by TAT. The increment in the quarter-chord moment about the

aerodynamic center due to a flap deflection δ_f is given by Eq. 2.17

$$\Delta C_{m_{c/4}} = \left[\frac{1}{4}\sin 2\theta_f - \frac{1}{2}\sin\theta_f\right]\delta_f \tag{2.17}$$

This equation provides the direct ability to either predict the moment changes due to flap deflection, or determine a flap setting which will produce a moment necessary for trim, and adds completeness when solving for reduced drag with a trim constraint.

2.1.4 Basic and Additional Lift Distributions

The goal of the current problem is to solve for the optimal flap angles of an adaptive tailless aircraft which minimizes drag and maintains longitudinal trim. An integral part of the solution presented in this thesis is the concept of basic and additional lift distributions, which is described in detail in several references.[26,27] Presented here is a brief description of the concepts that were utilized, which have been tailored with respect to the issues at hand, namely achieving a desired pitching moment for tailless aircraft. By using this method, simple analytical expressions can be derived which enable the ability to solve for the desired flap angles of a planar wing with multiple TE flaps.

If one maintains the assumptions of linear aerodynamics (linear $C_l - \alpha$ slope and linear $C_l - \Gamma$ relationship), then a wing's lift distribution can be divided into the sum of two parts: (i) basic lift and (ii) additional lift. Further, if the wing's chord distribution is provided then the C_l distribution of the wing can similarly be divided into the sum of two parts:

$$C_l = C_{lb} + C_{la} \tag{2.18}$$

The C_{lb} term in Eq. 2.18 refers the wing's basic lift distribution. This distribution is defined at wing $C_L = 0$, and describes the C_l distribution due to variations in geometric twist, aerodynamic twist, and flap deflection of the wing, as well as chord distribution. Geometric twist is achieved by twisting the wing so that the geometric angle-of-attack varies in the spanwise direction. Aerodynamic twist is determined by the spanwise variation in airfoil section, which is the difference in airfoil camber or maximum camber position across the span. Lastly, flap deflation describes a change in airfoil camber, but is set apart from aerodynamic twist for the purposes of this study. Because changes in each of these parameters (twist, camber, and flap deflection) cause linear shifts in their respective C_{lb} distributions, they can be summed and the resulting distribution describes total wing C_{lb}:

$$C_{lb} = C_{lb,twist} + C_{lb,camber} + C_{lb,flap} \tag{2.19}$$

The C_{la} term in Eq. 2.18 refers the wing's additional lift distribution. This distribution is defined with wing twist and flap deflection set to zero, and is determined by the wing's chord distribution. If a linear lift slope is assumed, the value of C_{la} at wing $C_L = 1$ can be precomputed and used to solve the C_{la} distribution for any C_L as follows:

$$C_{la} = C_L C_{la,1} \tag{2.20}$$

where $C_{la,1}$ is the C_l distribution of the wing at $C_L = 1$ and zero twist.

In order to illustrate this concept, a simple graphical description is provided here. Figure 2.5 displays the right-hand-side rear view of a planar, aft-swept, tapered wing which has five TE flaps that each have a flap-to-chord ratio of 0.2. The spanwise flap locations are labeled flap 1, flap 2, and so on. Shown in part (a)

of the figure are the basic lift distributions that result from separate flap deflections of five degrees for flap 1 and flap 2, labeled C_{lb_1} and C_{lb_2} respectively, as well as the $C_{la,1}$ distribution as computed by WINGS, a discrete-vortex Weissinger's method code. Part (b) of the figure represents a superposition of the curves from part (a), as well as a predicted solution from WINGS when flaps 1 and 2 have been deflected five degrees. Indicated by this example is the linear relationship between C_{lb} and C_{la} for the determination of C_l.

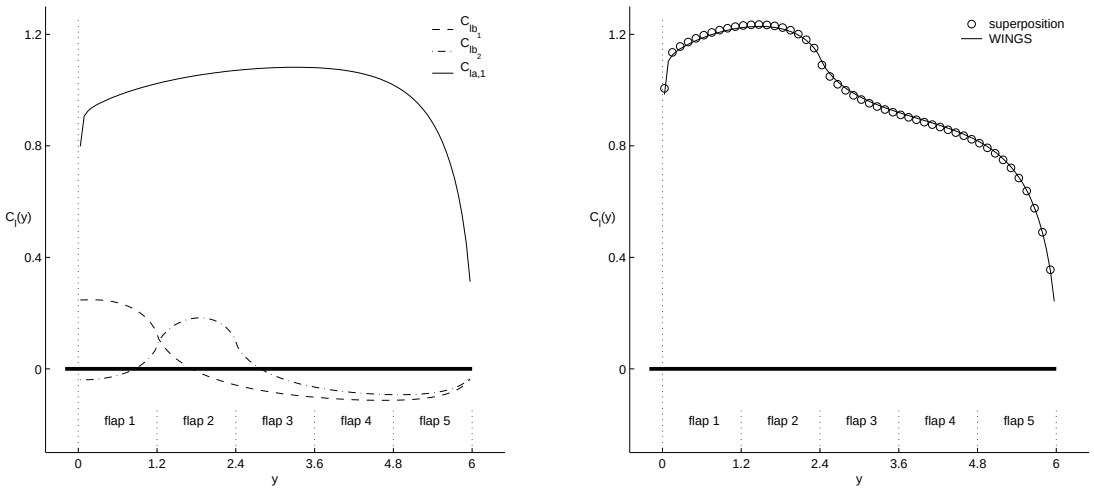

Figure 2.5: Lift distribution for a planar wing, (a) additional and basic lift and (b) C_l due to superposition in comparison to C_l from WINGS.

For tailless aircraft the C_{lb} and C_{la} distributions take on very significant and different roles with respect longitudinal trim. Presented in Fig. 1.3 is the layout of a hypothetical swept wing showing the location of the wing's aerodynamic center. In terms of pitching moment coefficient (C_M), the aerodynamic center of the wing is the location where C_M is independent of changes in α, and is labeled $C_{M_{ac}}$. This value is therefore independent of C_L, and is designed to be located aft of the aircraft center of gravity (X_{cg}) in order to achieve longitudinal static stability. The difference in X_{ac} and X_{cg} is universally known as the aircraft static margin, and is a design criteria for desired handling (longitudinal static stability). Because the

aerodynamic center is located at the centroid of the additional lift distribution, it follows that changes in C_{la} will not influence $C_{M_{ac}}$. Therefore, it is the C_{lb} distribution changes which will account for changes in $C_{M_{ac}}$ due to lift, which leads to the variable $\left(C_{M_{ac_w}}\right)_{basic}$, or the pitching moment coefficient resulting from the basic lift distribution. This variable will take on significant importance for the minimization of induced drag given a longitudinal trim constraint, and will be described fully in Sec. 2.2.1 and Sec. 2.2.2.

The decoupling of C_{lb} and C_{la} allows not only the ability to directly influence $C_{M_{ac}}$, it also has specific implications for constraining lift. Recall that C_{la} is the only part of the lift that scales with α, and thus C_L, as C_{lb} is defined at $C_L = 0$. And, since variations in C_{la} will not result in $C_{M_{ac}}$ changes, C_{la} can be used to achieve desired lift while C_{lb} can be used to achieve a desired $C_{M_{ac}}$. The linear relationship of C_{lb} and C_{la} plays an integral part for solving the current problem, as each part needs to be optimized with respect to the constraints in order to produce a solution.

2.2 Procedure

This section of the thesis describes the methodology used to solve the optimum flap angles for an adaptive tailless aircraft. First described is the breakdown of wing pitching moment, as a specific derivation of this term was used in the current research. Next, solutions pertaining to minimizing induced drag as the primary goal are discussed. Lastly, the methodology for the primary goal of minimal profile drag is addressed. In each case of drag minimization, the methods are derived for an arbitrary tailless aircraft with an undefined number of trailing edge flaps placed across its span. The constraints are longitudinal trim and lift.

2.2.1 Pitching Moment Definition

The focus of the current problem is to solve for the optimal flap distribution resulting in minimized drag for an adaptive tailless aircraft with multiple TE flaps. Perhaps the most important consideration when designing the lift distribution of a tailless aircraft is the resulting pitching moment, as trim implications cannot be ignored. And as shown in Sec. 2.1.1, the value $C_{M_{ac_w}}$ takes on the greatest significance for trim. This section provides the derivations used for defining the aircraft pitching moment about the ac with respect to two considerations: basic lift and spanwise airfoil sections. The pitching moment resulting from basic lift was introduced in Sec. 2.1.4, while the pitching moment due to spanwise airfoil sections will be introduced now. By considering these two terms separately, it becomes possible to utilize them as governing variables for the minimization of induced and profile drag.

The first step in understanding the pitching moment as defined for this work is to start with the general equation for the pitching moment of an aft-swept wing. Equation 2.4 previously presented this equation, and will now be restated in a more conventional, nondimentionalized form

$$C_{M_{ac_w}} = \frac{1}{S\bar{c}} \left\{ \int_{\frac{-b}{2}}^{\frac{b}{2}} C_{m_{ac}}(y) c(y)^2 dy + \int_{\frac{-b}{2}}^{\frac{b}{2}} C_{lb}(y) [X_{ac,wing} - X_{ac}(y)] c(y) dy \right\} \quad (2.21)$$

where S is the reference area of the wing, $\bar{c}$ is the mean aerodynamic chord of the wing, b is the wingspan, and $X_{ac,wing}$ as well as X_{ac} are as defined previously in Fig. 1.3. Wing pitching moment comes from two contributions: (1) airfoil pitching moment when integrated across the span, as indicated by the first term in the brackets on the RHS of Eq. 2.21, and (2) the moment due to the spanwise lift distribution along a swept quarter-chord line, as indicated by the second term in the brackets on the RHS of Eq. 2.21. For clarity, part (1) of Eq. 2.21 will be

referred to as $\left(C_{M_{ac_w}}\right)_{sections}$, while part (2) will be deemed $\left(C_{M_{ac_w}}\right)_{basic}$, allowing that equation to be rewritten as a simple linear combination of the two terms, as indicated by Eq. 2.22.

$$C_{M_{ac,wing}} = \left(C_{M_{ac_w}}\right)_{sections} + \left(C_{M_{ac_w}}\right)_{basic} \tag{2.22}$$

The terms $\left(C_{M_{ac_w}}\right)_{sections}$ and $\left(C_{M_{ac_w}}\right)_{basic}$ are now expanded to suit the current problem and to display the significance of each.

The first contribution to pitching moment as discussed above is that due to the airfoil sections, labeled $\left(C_{M_{ac_w}}\right)_{sections}$. The effects of this term will be the result of two considerations, the design of the spanwise airfoil sections and the angle of flap deflections for the multiple TE flap system. The expanded version takes the following form:

$$\left(C_{M_{ac_w}}\right)_{sections} = \frac{1}{S\bar{c}} \left\{ \begin{array}{c} 2\int_0^{\frac{b}{2}} C_{m_{ac}}(y)c(y)^2 dy + \\ \left(2\int_0^{y_1} C_{m_{\delta_{f_1}}} dy\right)\delta_{f_1} + ... + \left(2\int_{y_{N-1}}^{y_N} C_{m_{\delta_{f_N}}} dy\right)\delta_{f_N} \end{array} \right\} \tag{2.23}$$

where N is the number of TE flaps distributed across the wing half span such that the flap spanwise location extends from y_{N-1} to y_N, $C_{m_{\delta_{f_N}}}$ represents the additional moment coefficient to the airfoil sections resulting from a deflection of the N^{th} flap, and δ_{f_N} is the angle of deflection of flap N. The factor of 2 preceding each integral indicates lateral symmetry. Through use of this equation, the created variable $\left(C_{M_{ac_w}}\right)_{sections}$ can be computed for any given planform, airfoil distribution, and series of flap deflections.

The second contribution to wing pitching moment as described above is that due to the lift distribution when integrated across the span of a swept quarter-chord, and is labeled $\left(C_{M_{ac_w}}\right)_{basic}$. As stated in Sec. 2.1.4, the only portion of the lift that is going to affect the pitching moment is the basic lift, hence the subscript

basic. Referring again to Sec. 2.1.4, it was stated that basic lift will be linearly affected by three factors: geometric twist, aerodynamic twist, and flap deflection (subscripted twist, camber, and δ_f). These are the three occurrences that make up the expanded version of Eq. 2.24, where C_{lb} is the basic lift coefficient due to each of the three occurrences.

$$\left(C_{M_{ac_w}}\right)_{basic} = \frac{1}{S\bar{c}} \left\{ \begin{array}{c} 2\int_0^{\frac{b}{2}} C_{lb,twist}(X_{ac,w} - X_{ac}(y))c(y)dy + \\ 2\int_0^{\frac{b}{2}} C_{lb,camber}(X_{ac,w} - X_{ac}(y))c(y)dy + \\ \left(2\int_0^{\frac{b}{2}} C_{lb,\delta_{f_1}}(X_{ac,w} - X_{ac}(y))c(y)dy\right)\delta_{f_1} + ... + \\ \left(2\int_0^{\frac{b}{2}} C_{lb,\delta_{f_N}}(X_{ac,w} - X_{ac}(y))c(y)dy\right)\delta_{f_N} \end{array} \right\} \tag{2.24}$$

By solving the basic lift distribution of any given planform, Eq. 2.24 can be used to solve for the resulting change to pitching moment.

As stated previously, a linear combination of these two terms provides the solution of aircraft pitching moment about the aerodynamic center, as shown in Eq. 2.22. It is necessary to tailor the value of $C_{M_{ac,wing}}$ with respect to the locations of aerodynamic center and center of gravity in order to produce a desired static margin and maintain positive handling qualities. The ability to vary either $\left(C_{M_{ac_w}}\right)_{basic}$ or $\left(C_{M_{ac_w}}\right)_{sections}$ for this purpose has been introduced, however each term is dependent on the TE flap angle distribution which leads to difficulties. In order to overcome these difficulties, a novel approach was employed which effectively separates the two terms. The central idea of this approach is the introduction of a "mean" flap term, $\bar{\delta}_f$.

Previous adaptive wing studies[1] have shown benefits for defining the TE flap angle distribution ($\{\delta_f\}$) of the wing as the sum of two parts: (1) a constant flap angle (close to the mean flap angle), $\bar{\delta}_f$, and (2) the variation about the mean, $\left\{\hat{\delta}_f\right\}$. This relationship is displayed in Eq. 2.25, where the curly brackets signify $N\times1$ matrices with N being the number of TE flaps distributed along the

half-span, and $\bar{\delta}_f$ is a constant.

$$\{\delta_f\} = \bar{\delta}_f + \left\{\hat{\delta}_f\right\} \tag{2.25}$$

By extracting a constant value from the flap distribution, specific consequences result with respect to the pitching moment. These consequences will aid in essentially decoupling $\left(C_{M_{ac_w}}\right)_{basic}$ and $\left(C_{M_{ac_w}}\right)_{sections}$, allowing for each to be varied independently for specifying $C_{M_{ac,wing}}$ and achieving a desired static margin.

The constant flap is essentially a full-span flap, and can be set to any constant angle. Because $\bar{\delta}_f$ acts as a full span flap, it takes on certain characteristics of benefit to the problem at hand. Deflecting a full-span TE flap is comparable to deflecting a TE flap in 2-D, and produces similar results. Notably, a deflection of $\bar{\delta}_f$ creates a shift in the $C_l - \alpha$ curve, which is comparable to a change in α. It was presented previously in Sec. 2.1.4 that changes in α affect only the additional lift distribution, and has no affect on the basic lift distribution. And, it is important to recall that the basic lift is the lift which effects $C_{M_{ac,wing}}$. As a result, $\bar{\delta}_f$ will have no affect on $\left(C_{M_{ac_w}}\right)_{basic}$ provided $\left\{\hat{\delta}_f\right\}$ is unchanged. The constant flap will, however, influence $\left(C_{M_{ac_w}}\right)_{sections}$ as a full span flap deflection leads to a shift in the pitching moment curve as well. Thus, $\bar{\delta}_f$ can be set to tailor $\left(C_{M_{ac_w}}\right)_{sections}$ without affecting $\left(C_{M_{ac_w}}\right)_{basic}$, providing the direct ability to solve for a desired value of $C_{M_{ac,wing}}$.

Presented now are redefined, expanded versions of the $\left(C_{M_{ac_w}}\right)_{basic}$ and $\left(C_{M_{ac_w}}\right)_{sections}$ equations originally found in Eqs. 2.23 and 2.24. The new equations make use of Eq. 2.25 for redefining $\{\delta_f\}$ and highlight the effect that $\bar{\delta}_f$ has on each. It should be noticed that $\bar{\delta}_f$ appears only in the $\left(C_{M_{ac_w}}\right)_{sections}$ equation, as it will have no affect on $\left(C_{M_{ac_w}}\right)_{basic}$, as discussed previously. However, because $\left\{\hat{\delta}_f\right\}$ appears in both terms there is certian amount of dependance that $\left(C_{M_{ac_w}}\right)_{basic}$

has on $\left(C_{M_{ac_w}}\right)_{sections}$, and is evident when solving for minimum profile drag, as discussed in Sec. 2.2.3.

$$\left(C_{M_{ac_w}}\right)_{sections} = \frac{1}{S\bar{c}} \left\{ \begin{array}{c} 2\int_0^{\frac{b}{2}} C_{m_{ac}}(y)c(y)^2 dy + \\ \left(2\int_0^{\frac{b}{2}} C_{m_{\bar{\delta}_f}} dy\right)\bar{\delta}_f + \\ \left(2\int_0^{y_1} C_{m_{\hat{\delta}_{f_1}}} dy\right)\hat{\delta}_{f_1} + ... + \left(2\int_{y_{N-1}}^{y_N} C_{m_{\hat{\delta}_{f_N}}} dy\right)\hat{\delta}_{f_N} \end{array} \right\} \quad (2.26)$$

$$\left(C_{M_{ac_w}}\right)_{basic} = \frac{1}{S\bar{c}} \left\{ \begin{array}{c} 2\int_0^{\frac{b}{2}} C_{lb,twist}(X_{ac,w} - X_{ac}(y))c(y)dy + \\ 2\int_0^{\frac{b}{2}} C_{lb,camber}(X_{ac,w} - X_{ac}(y))c(y)dy + \\ \left(2\int_0^{\frac{b}{2}} C_{lb,\hat{\delta}_{f_1}}(X_{ac,w} - X_{ac}(y))c(y)dy\right)\hat{\delta}_{f_1} + ... + \\ \left(2\int_0^{\frac{b}{2}} C_{lb,\hat{\delta}_{f_N}}(X_{ac,w} - X_{ac}(y))c(y)dy\right)\hat{\delta}_{f_N} \end{array} \right\} \quad (2.27)$$

$\left(C_{M_{ac_w}}\right)_{basic}$ and $\left(C_{M_{ac_w}}\right)_{sections}$ become powerful tools for solving the longitudinal trim constraint enforced by the current problem. And by carefully selecting $\bar{\delta}_f$, they also become an integral part for reducing drag, as will be shown in upcoming sections.

2.2.2 Induced Drag Reduction as Primary Goal (Scheme A)

As stated in Sec. 2.1.2, minimum induced drag is a result of the familiar elliptical loading for a planar wing. Presented in the same section was the methodology for determining the lift distribution resulting in minimized induced drag with a constraint on the pitching moment contributed by the lift distribution. This lift will be labeled $C_{l,desired}$ as it represents the lift to be matched in order to achieve minimum induced drag. By use of $C_{l,desired}$, and the basic (C_{lb}) and additional (C_{la}) lift coefficients presented in Sec. 2.1.4, a linear relationship can be formed for solving the flap deflections resulting in desired C_l.

$$C_L \{C_{la,1}\} + \{C_{lb,twist}\} + \{C_{lb,camber}\} + [C_{lb,f}]\{\delta_f\} = \{C_{l,desired}\} \quad (2.28)$$

Equation 2.28 displays the resulting linear system of equations, where the curly brackets again signify $N \times 1$ matrices with N representing the number of flaps distributed along the half-span. The matrix $\{\delta_f\}$ represents the flap angles that will produce a lift distribution that matches $\{C_{l,desired}\}$, which was determined by interpolating the $C_{l,desired}$ distribution at control sections equating to the spanwise flap locations. Further, because $\bar{\delta}_f$ was defined with the ability to take on any value, the $\{\delta_f\}$ in Eq. 2.28 can be substituted with $\left\{\hat{\delta}_f\right\}$. Noting that $[C_{lb,f}]$ is singular, an additional equation is required to solve for $\left\{\hat{\delta}_f\right\}$ and that equation, Eq. 2.29, is simply a statement that the weighted-mean of $\left\{\hat{\delta}_f\right\}$ is zero.

$$S_{f_1}\hat{\delta}_{f_1} + S_{f_2}\hat{\delta}_{f_2} + ... + S_{f_N}\hat{\delta}_{f_N} = 0 \tag{2.29}$$

where S_{f_1}, S_{f_2}, ... S_{f_N} are the areas of the wing occupied by the respective flaps.

By finding $\left\{\hat{\delta}_f\right\}$, a numerical solution to the flap settings has been achieved which results in minimized induced drag with respect to a pitching moment constraint, which is equal to the value of $\left(C_{M_{ac_w}}\right)_{basic}$. However, if truly minimal induced drag is desired, then elliptical loading is necessary despite the pitching moment effects, forcing special consideration. It becomes necessary to determine the value of $\left(C_{M_{ac_w}}\right)_{basic}$ that corresponds to elliptical loading.

It is known from wing theory that for elliptical loading, the spanwise location of the center of loading can be found using the following relation:

$$Y_{cp} = \left(\frac{4}{3\pi}\right)\left(\frac{b}{2}\right) \tag{2.30}$$

where b is the wingspan. It is a simple matter to then subtract this value from the spanwise aerodynamic center location ($Y_{ac,wing}$ in Fig. 1.3) and multiply by lift and $\tan(\Lambda)$ (Λ is the sweep angle) to determine the pitching moment about the aero-

dynamic center which results from elliptical loading, and is labeled $\left(C_{M_{ac_w}}\right)_{basic}^{elliptic}$ in Eq. 2.31.

$$\left(C_{M_{ac_w}}\right)_{basic}^{elliptic} = \frac{C_L}{c_{ref}} \left[Y_{ac,wing} - Y_{cp}\right] \tan(\Lambda) \tag{2.31}$$

By constraining $\left(C_{M_{ac_w}}\right)_{basic}$ with this moment value, it is possible to solve for $\left\{\hat{\delta}_f\right\}$ which produces elliptical loading. Although resulting in minimum induced drag, this moment is not sufficient to satisfy the constraint of trim. Thus, it is necessary to utilize $\left(C_{M_{ac_w}}\right)_{sections}$ to result in desired handling qualities.

As was previously discussed, $\bar{\delta}_f$ can be used to directly tailor $\left(C_{M_{ac_w}}\right)_{sections}$ without effecting $\left(C_{M_{ac_w}}\right)_{basic}$. This fact is useful now, as $\left(C_{M_{ac_w}}\right)_{basic}$ has been constrained to ensure elliptical loading, leaving $\left(C_{M_{ac_w}}\right)_{sections}$ responsible for ensuring trim. Given a desired SM, $C_{M_{ac,wing}}$ is known and $\left(C_{M_{ac_w}}\right)_{sections}$ can be determined using Eq. 2.22. It is a simple matter to then determine $\bar{\delta}_f$ which results in the proper $\left(C_{M_{ac_w}}\right)_{sections}$ value, and the longitudinal trim constraint is satisfied while maintaining minimum induced drag. The α for the desired lift is then determined through iteration. Thus, both trim and lift are achieved.

By following these steps, it is possible to create a flying wing that maintains elliptical loading (minimum induced drag), longitudinal trim, and desired lift. It should be noted that no constraints were placed on the value of the flap setting or on α. It is assumed that the airfoil design, twist distribution, etc., of an aircraft using this system will be such that extreme flap angles will not be necessary. Minimizing induced drag is typically desirable at high-C_L flight conditions such as long-range and endurance cruise climb.

Provided in Fig 2.6 is a flowchart representing the drag reduction scheme presented above. This method of drag reduction is referred to as *Scheme A* in the results chapter.

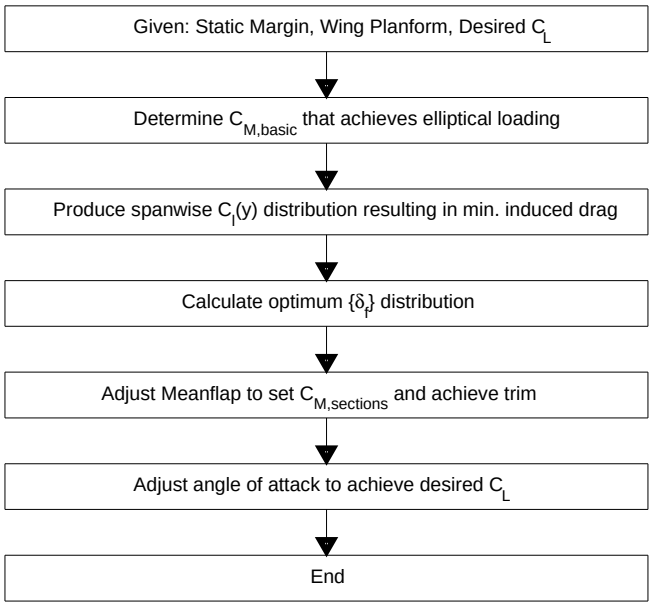

Figure 2.6: Flowchart for *Scheme A*.

2.2.3 Profile Drag Reduction as Primary Goal (Scheme B)

To solve for the optimal flap angles with respect to profile drag reduction, similar methodology is used. The difference in the two schemes is that where previously $\left(C_{M_{ac_w}}\right)_{basic}$ was determined from the need for elliptical loading and $\left(C_{M_{ac_w}}\right)_{sections}$ was tailored in order to achieve trim, now it is desired to first set $\bar{\delta}_f$ so that the majority of the wing is operating in the LDR, thus reducing profile drag and determining $\left(C_{M_{ac_w}}\right)_{sections}$, while using $\left\{\hat{\delta}_f\right\}$ for achieving trim and minimal induced drag with a pitching moment constraint of $\left(C_{M_{ac_w}}\right)_{basic}$. The control variable for this effort becomes $\left(C_{M_{ac_w}}\right)_{sections}$.

It is first necessary to determine the methodology for setting the $\bar{\delta}_f$ as to

reduce profile drag. It was already discussed in Sec. 2.1.3 that for an NLF airfoil, the maintenance of laminar flow across the upper and lower surfaces results in optimal stagnation point location, and thus operation in the airfoil LDR. Because $\bar{\delta}_f$ has characteristics of a 2-D trailing edge flap, it can thus be set accordingly for placing the stagnation point in an optimal location.

The mean flap angle is set using a combination of past adaptive wing procedures and TAT relations, and can be determined using:

$$\bar{\delta}_f = \frac{C_L - C_{Lideal}}{2\sin\theta_f} \tag{2.32}$$

where C_{Lideal} is the C_L corresponding to a point within the LDR of the unflapped airfoil being used, and $2\sin\theta_f$ is gathered from TAT and represents the C_l-shift in the drag bucket due to a one-radian flap deflection. C_{Lideal} is determined using the following equation:

$$C_{Lideal} = \frac{2}{S}\int_0^{\frac{b}{2}} c(y)C_{lideal}(y)dy \tag{2.33}$$

By using the preceding equations, $\bar{\delta}_f$ can be set and Eq. 2.26 can be used to calculate $\left(C_{M_{ac_w}}\right)_{sections}$ with the variation flap distribution, $\left\{\hat{\delta}_f\right\}$, set to zero. Through knowledge of the desired static margin, it is then possible to calculate the moment required from the lift distribution and thus find the desired value of $\left(C_{M_{ac_w}}\right)_{basic}$. The methodology presented in Sec. 2.1.2 is then used to determine the C_l distribution that results in required pitching moment and minimum induced drag, and $\left\{\hat{\delta}_f\right\}$ is then determined using Eq. 2.28. It should be noted that because $\left\{\hat{\delta}_f\right\}$ exists in both the $\left(C_{M_{ac_w}}\right)_{basic}$ and $\left(C_{M_{ac_w}}\right)_{sections}$ terms, once the variation flap angles are solved for a change to $\left(C_{M_{ac_w}}\right)_{sections}$ will occur. However, proper airfoil design leads this change to be of slight magnitude, and can be resolved

through minimal iterations of the procedure presented above. And, if an iterative precess is undesirable, it is possible to make a small variation to $\bar{\delta}_f$ as to counteract the moment variation, as proper design of the airfoil used should provide a LDR large enough to accommodate such a small change.

Provided in Fig 2.7 is a flowchart representing the drag reduction scheme presented above. This method of drag reduction is referred to as *Scheme B* in the results chapter.

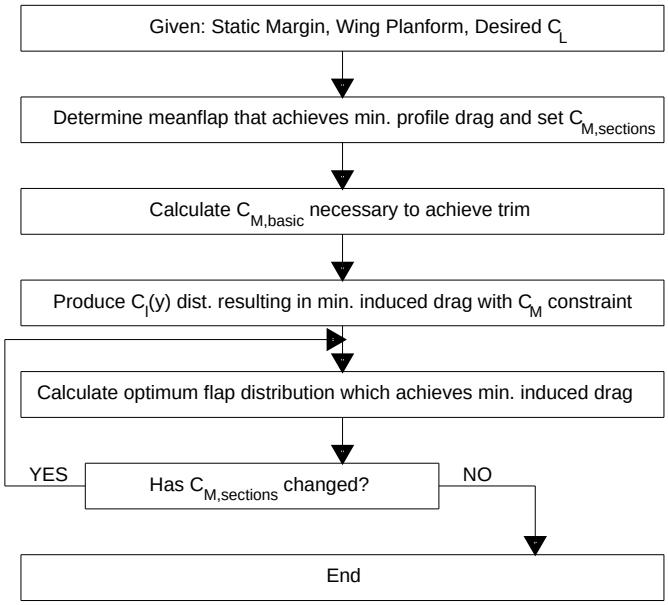

Figure 2.7: Flowchart for *Scheme B*.

Chapter 3

Results

This section of the thesis describes results obtained when implementing the theory derived in Sec. 2.2 on a tailless aircraft which has a planar wing configuration and utilizes multiple TE flaps for the purpose of wing adaptation. Presented first are the relationships between drag reduction with respect to induced drag as the primary goal and also with respect to profile drag as the primary goal. Next are discussions pertaining to the effects that sweep and airfoil pitching moment coefficient have on the problem of reducing drag with a trim constraint. Lastly, a short study of static margin change is presented. A summary of all results is provided in Chapter 4.

3.1 Test Cases

The results presented here were derived from specific cases selected to analyze the effects of targeting drag reduction with respect to induced drag and profile drag. Also selected were cases displaying the affect sweep change as well as airfoil section pitching moment coefficient change have for drag reduction. These cases were selected due to the influence that sweep has on $\left(C_{M_{ac_w}}\right)_{basic}$ and the influence that airfoil section pitching moment coefficient has on $\left(C_{M_{ac_w}}\right)_{sections}$, as these terms were described to be governing variables for the current problem in Secs. 2.2.1–

2.2.3.

In order to test the methodology derived in this thesis, a hypothetical tailless aircraft was used as the example platform with characteristics displayed in Table 3.1. As shown, certain parameters were varied, namely quarter-chord sweep angle and airfoil section, in order to provide test cases pertaining to the specific methods used for drag reduction and trim. The aircraft weight (W) along with flight C_L were used to solve for Reynolds number at each flap section location across the span of the tapered wing in order to more accurately predict the effects of the flap deflections. As shown, the aircraft static margin was chosen to be 10% of the mean aerodynamic chord. For each case, the number of TE flaps along the wing half span was selected to be five, with each flap maintaining a flap-to-chord ratio of 0.2. Figure 3.1 displays the planform of this aircraft when $\Lambda = 20$ deg and shows the equally-spaced TE flaps.

Table 3.1: Assumed parameter values for example hypothetical tailless aircraft.

Static Parameters	Value
Gross weight (W)	14,200 N (3,200 lbf)
Mean aerodynamic chord ($\bar{c}$)	1.01 m (3.31 ft)
Reference area (S)	12.0 m^2 (130 ft^2)
Wing aspect ratio (AR)	12
Static margin (SM)	10 % $\bar{c}$
Number of half-span TE flaps (N)	5
Flap-to-chord ratio (all flaps)	0.2
Variable Parameters	**Value**
$\frac{1}{4}$ *chord* sweep angle (Λ)	20 deg 35 deg
Airfoil section	$CAMBERED$ ($C_{m_0} = -0.0802$) $REFLEXED$ ($C_{m_0} = 0.055$)

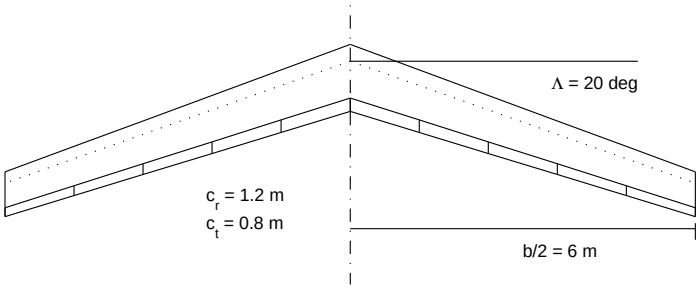

Figure 3.1: Example planform for Λ equal to 20 degrees and 5 TE flaps per half span.

Information is presented regarding the two different airfoil sections that were utilized to study the effects that airfoil section pitching moment has on the reduction of drag with respect to trim. The first airfoil is a cambered NLF airfoil which has a zero lift pitching moment coefficient (C_{m_0}) of -0.0802, and is labeled $CAMBERED$. This airfoil was selected due to its well defined low drag range, or drag bucket, which surrounds the C_l value of 0.5. The second airfoil is a reflexed airfoil which was designed to have a positive C_{m_0} value of 0.055, and is named $REFLEXED$. It was decided to study an airfoil of this type because often times reflexed airfoils are utilized on tailless aircraft due to the need for positive lift while also maintaining near zero, or positive, pitching moment. Each of these airfoils were created using the multipoint inverse airfoil design method PROFOIL,[28,29] which allows for the specification of airfoil C_{m_0} as a design parameter. Figures 3.2 and 3.3 display the properties of these airfoils as predicted by XFOIL[30] calculated at a $Re\sqrt{C_l}$ of three million, as well as their corresponding geometries. It should be noted that care was taken in the design of the $REFLEXED$ airfoil to place the center of the drag bucket at $C_l = 0.5$ in an attempt to mimic the lift and drag properties of the $CAMBERED$ airfoil. By doing so, it is assumed that more accurate comparisons can be made between the airfoils pertaining to drag reduction as well as sweep angle and C_{m_0} influence with respect to trim.

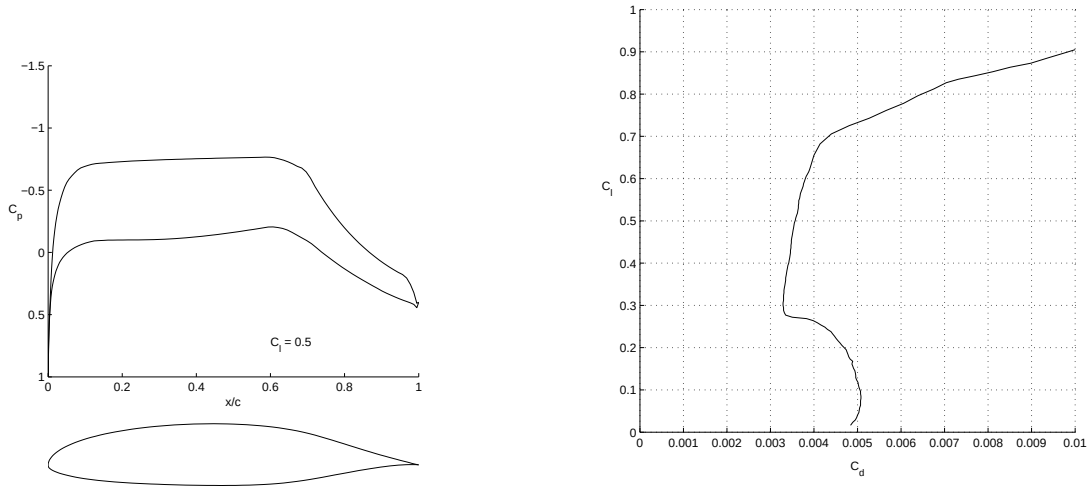

(a) (b)

Figure 3.2: $CAMBERED$ airfoil: (a) Geometry and C_p distribution, and (b) drag polar at $Re\sqrt{C_l}$ three million.

As previously stated, the two airfoils whose aerodynamic properties are displayed in Figs 3.2 and 3.3 were utilized for the wing planform shown in Fig. 3.1 at sweep angles of 20 deg and 35 deg. This results in four specific configurations, which are presented here as example cases. Example Case #1 is the $CAMBERED$ airfoil at $\Lambda = 20$ deg and is presented in Sec. 3.1.1. Example Case #2 is the $CAMBERED$ airfoil at $\Lambda = 35$ deg and is presented in Sec. 3.1.2. Example Case #3 is the $REFLEXED$ airfoil at $\Lambda = 20$ deg and is presented in Sec. 3.1.3. Example Case #4 is the $REFLEXED$ airfoil at $\Lambda = 35$ deg and is presented in Sec. 3.1.4. For each of these cases the methodology which focuses on induced drag minimization as the primary goal and the methodology which focuses on profile drag minimization as the primary goal were both tested for a range of C_l values in order to spawn comparisons. The application of these methodologies have been labeled *Scheme A* and *Scheme B* respectively, and descriptions of each are listed here for clarity.

Scheme A : This represents the methodology presented in Sec. 2.2.2, where the primary focus is the achievement of minimum induced drag through the

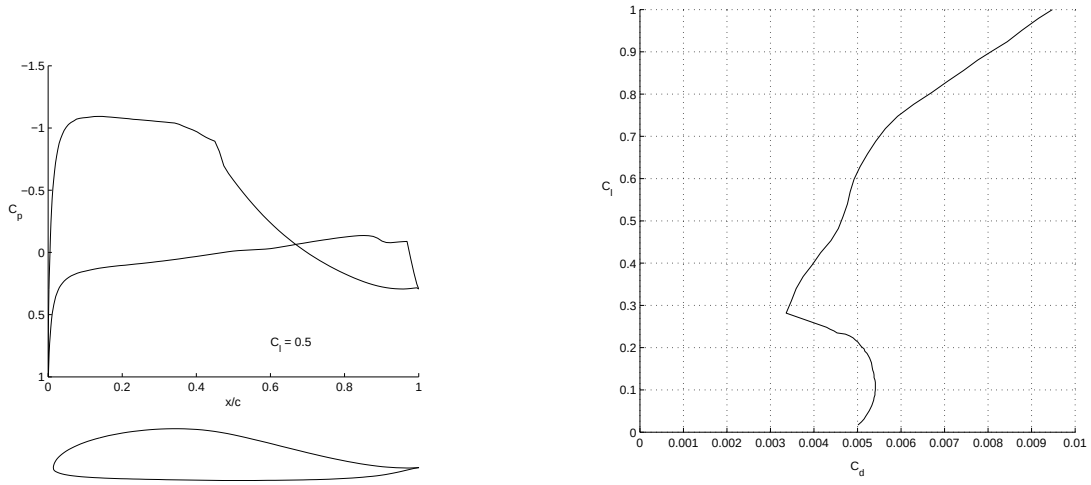

(a) (b)

Figure 3.3: $REFLEXED$ airfoil: (a) Geometry and C_p distribution, and (b) drag polar at $Re\sqrt{C_l}$ three million.

generation of elliptical loading. In this scheme, the moment about the wing ac produced by elliptical loading is determined and constrains the value of $\left(C_{M_{ac_w}}\right)_{basic}$. The spanwise variation flaps ($\hat{\delta}_f$) are then set accordingly to produce the optimal lift distribution. Next, the meanflap ($\bar{\delta}_f$) is chosen as to set the value of $\left(C_{M_{ac_w}}\right)_{sections}$ resulting in a pitching moment about the wing ac that was calculated to result in trim. This value is determined using the desired static margin, C_L, and longitudinal trim requirement which has $C_{M_{cg}} = 0$. It is evident that while this scheme results in minimum induced drag, the magnitude of $\bar{\delta}_f$ is unconstrained, allowing for the possibility that the wing sections are not operating within the low-drag range (LDR). The addition of the induced drag and profile drag components make up the total drag produced by this scheme.

Scheme B : This represents the methodology presented in Sec. 2.2.3, where the primary focus is on minimizing profile drag by determining the flap settings that enable the wing sections to operate in their respective low-drag-ranges, thereby reducing skin friction drag. A secondary focus is the determination

of the spanwise lift distribution which results in optimal induced drag with the constraint on the pitching moment such that the aircraft is trimmed longitudinally. In this scheme, the meanflap value ($\bar{\delta}_f$) is set as to ensure the spanwise wing sections are operating in the LDR, providing the initial value of $\left(C_{M_{ac_w}}\right)_{sections}$. Next, the value of $\left(C_{M_{ac_w}}\right)_{basic}$ is determined based on the calculated value of $C_{M_{ac_w}}$ that results in longitudinal trim. The value of $C_{M_{ac_w}}$ is determined using the desired static margin, C_L, and longitudinal trim requirement which has $C_{M_{cg}} = 0$. $\left(C_{M_{ac_w}}\right)_{basic}$ is used as a constraint to determine the spanwise lift distribution resulting in optimal induced drag, and the variation flap ($\hat{\delta}_f$) distribution is chosen accordingly. Any effect that the $\hat{\delta}_f$ distribution has on $\left(C_{M_{ac_w}}\right)_{sections}$ is calculated, and $\left(C_{M_{ac_w}}\right)_{basic}$ is adjusted through iteration to offset these effects, resulting in an iterative process which proceeds until longitudinal trim is achieved. It is evident that in this scheme profile drag is minimal, however the value of $\left(C_{M_{ac_w}}\right)_{basic}$ is unconstrained, allowing for the probability of increased induced drag because the lift distribution may be far from elliptical loading. Again, the addition of the induced drag and profile drag components make up the total drag produced by this scheme.

In each case the resulting distributions and drag numbers were obtained from a scripted process which utilized the 2-D flow solver XFOIL and the vortex-lattice code WINGS. Due to the theoretical nature of the methods applied, as well as the utilization of multiple codes in solving this problem, it became necessary to iterate the final solution in each case in order to ensure longitudinal trim. The requirement chosen for this iteration was wing pitching moment coefficient, and the process was halted once the magnitude of this value fell below 0.001. This value represents a moment produced by less then $\frac{1}{10}th$ of a meanflap deflection, and most often required only two iterations to satisfy.

3.1.1 Example Case #1

The first case discussed is the $CAMBERED$ airfoil used on the tapered wing planform with a sweep angle of 20 deg. Presented are the total drag numbers for the two drag reduction schemes tested where, as previously stated, the total drag number is produced through the addition of the induced and profile components of drag for each scheme. These values of total drag are plotted verses a range C_L values, highlighting how a lift constraint affects each method.

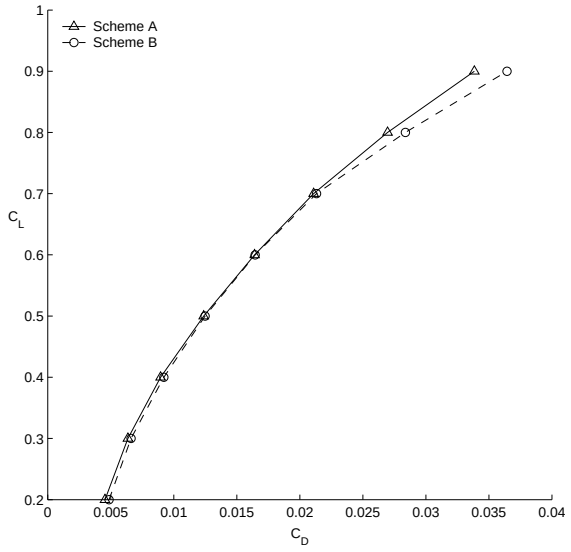

Figure 3.4: Comparison of total drag resulting from *Scheme A* and *Scheme B* for Example Case #1.

Spanwise results for three C_L values of 0.2, 0.5, and 0.8 are displayed in Figs. 3.5 and 3.6 for each of the schemes. In these plots, the circles indicate the target spanwise C_l distributions which result in minimum induced drag given pitching moment constraint and desired lift. The solid spanwise lines are the C_l distributions that were achieved by the methodology derived in the preceding sections, with flap angles represented at the upper portion of each flap section as indicated by the vertical dotted lines. A comparison of these lines give an indica-

tion of how well the flap distribution is minimizing induced drag. The meanflap used for trim is presented in the lower left hand corner of the plot for each C_L case. Overlaid each flap section is the drag polar ($C_d - C_l$ plot) as predicted by XFOIL for each of the five flaps. This gives a good indication of how well the flap settings are minimizing skin friction, or profile drag, as it is evident whether or not the section is operating in or near the drag bucket.

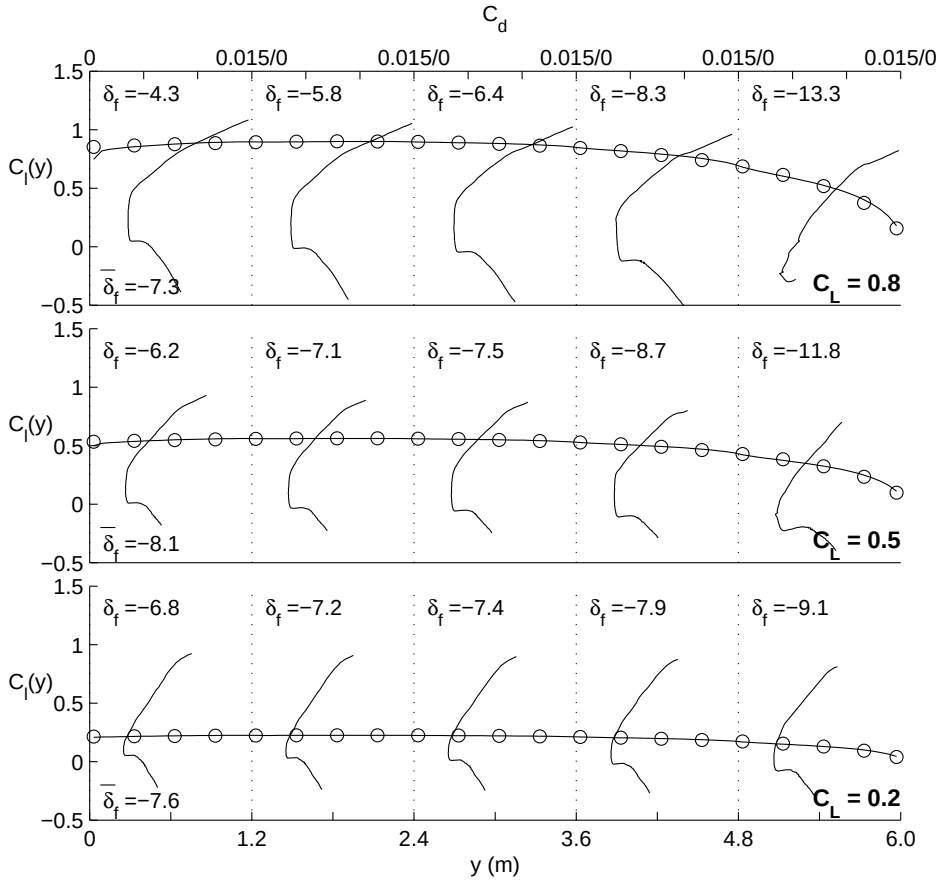

Figure 3.5: Spanwise C_l distributions with flap-section drag polars and optimal C_l distributions. Provided for C_L values of 0.2, 0.5, and 0.8 where *Scheme A* is applied.

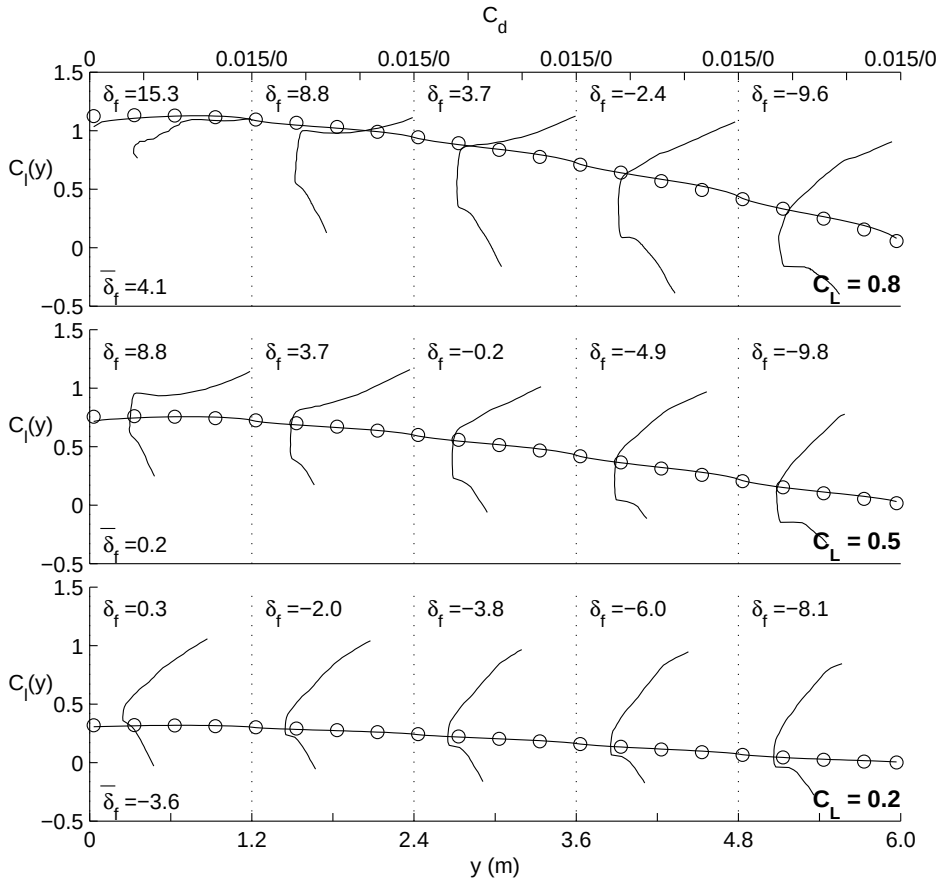

Figure 3.6: Spanwise C_l distributions with flap-section drag polars and optimal C_l distributions. Provided for C_L values of 0.2, 0.5, and 0.8 where *Scheme B* is applied.

In analyzing of Fig 3.5, it is evident that for all C_L values elliptical loading is achieved leading to minimum induced drag. However, it is also clear that in each C_L case the drag buckets are pushed to lower values, a result of the strong negative setting of $\bar{\delta}_f$, which determines the value of $\left(C_{M_{ac_w}}\right)_{sections}$ needed to offset $\left(C_{M_{ac_w}}\right)_{basic}$ produced by the elliptical loading. It is clear for this case that while minimum induced drag is achieved, there will be some penalties incurred in profile drag when trim is achieved. Total drag results are presented in Fig 3.4 and are labeled *Scheme A*.

The curve in Fig. 3.4 labeled *Scheme B* relates to Fig. 3.6, and provide similar results to those described above. These figures represent the C_L cases for the scheme in which profile drag reduction is the goal. As evident from this portion of the plot, for each C_L case the spanwise C_l distribution falls largely within the drag bucket, resulting in minimal values of profile drag; differing from what was seen in Fig. 3.5. The other striking difference is in the shape of the lift distribution produced by the flap settings. No longer will the C_l distribution result in elliptical loading, as it was necessary to vary it in order to achieve trim. In each C_L case the lift takes on a more bell-shaped distribution, which is typical of tailless aircraft. Again, the optimal target C_l distribution is plotted to provide a comparison with the achieved distribution which minimized induced drag with respect to the pitching moment constraint necessary for trim. In this case the inboard flaps for the C_L 0.8 case required a large deflection in order to achieve desired lift. This resulted in flow separation, as a result of which, a distinct drag bucket is absent.

Recalling the total drag curves displayed in Fig. 3.4, insight has been provided into how they were produced. By comparing the two curves, one can conclude that for this example case *Scheme A* generally results in minimum total drag. Thus, most important to this particular configuration is the achievement of elliptical loading despite the profile drag penalties.

3.1.2 Example Case #2

This example utilizes the same airfoil as Sec. 3.1.1, namely the $CAMBERED$ airfoil, along with the same planar, tapered configuration. However, this case was run at a sweep angle of 35 deg, which is more typical of tailless aircraft. Presented in Fig. 3.7 are total drag results similar to those shown in Example Case #1 while the spanwise lift results of Figs. 3.8 and 3.9 also mimic those above. Thus, for

this example and the similar upcoming examples, only brief discussions of these plots are provided.

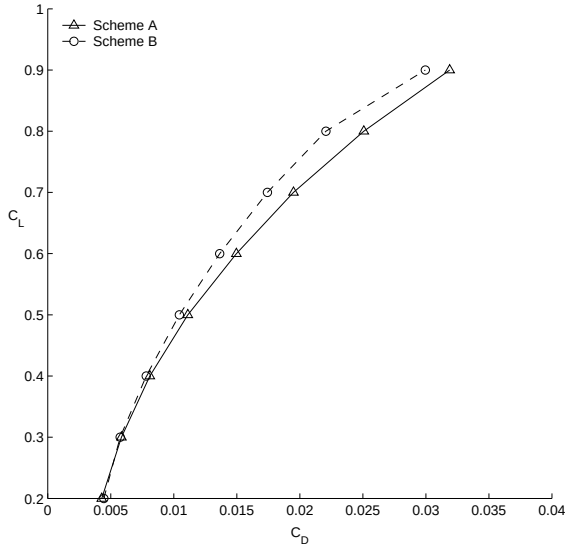

Figure 3.7: Comparison of total drag resulting from *Scheme A* and *Scheme B* for Example Case #2.

In this example, total drag reduction is largely achieved by *Scheme B*, a result opposite of that found in Sec. 3.1.1. This can be explained if one considers the spanwise C_l distributions shown in Fig. 3.8 and compares it with the distributions of Fig. 3.9. Recall that Fig. 3.8 is produced by *Scheme A* and results in elliptical loading. The previous example showed a more bell-shaped curve when *Scheme B* was applied, indicating increased values of induced drag compared to those produced by *Scheme A*. For this example, however, the curves in Fig. 3.9 are not obviously bell-shaped, and take a shape similar to those in Fig. 3.8. This leads to each case having similar induced drag numbers as those in Fig. 3.8. Figure 3.9, however, does mimic earlier results in that the majority of the sections are operating in the drag bucket, resulting in minimal profile drag. Because induced drag for both will be similar, we see that profile drag dominates this case, and thus the behavior of total drag seen in Fig. 3.7 which has *Scheme B* beneficial for this

configuration. A discussion of this finding is provided later in Sec. 3.2, as it can be shown that the sweep of the wing is largely responsible for this result.

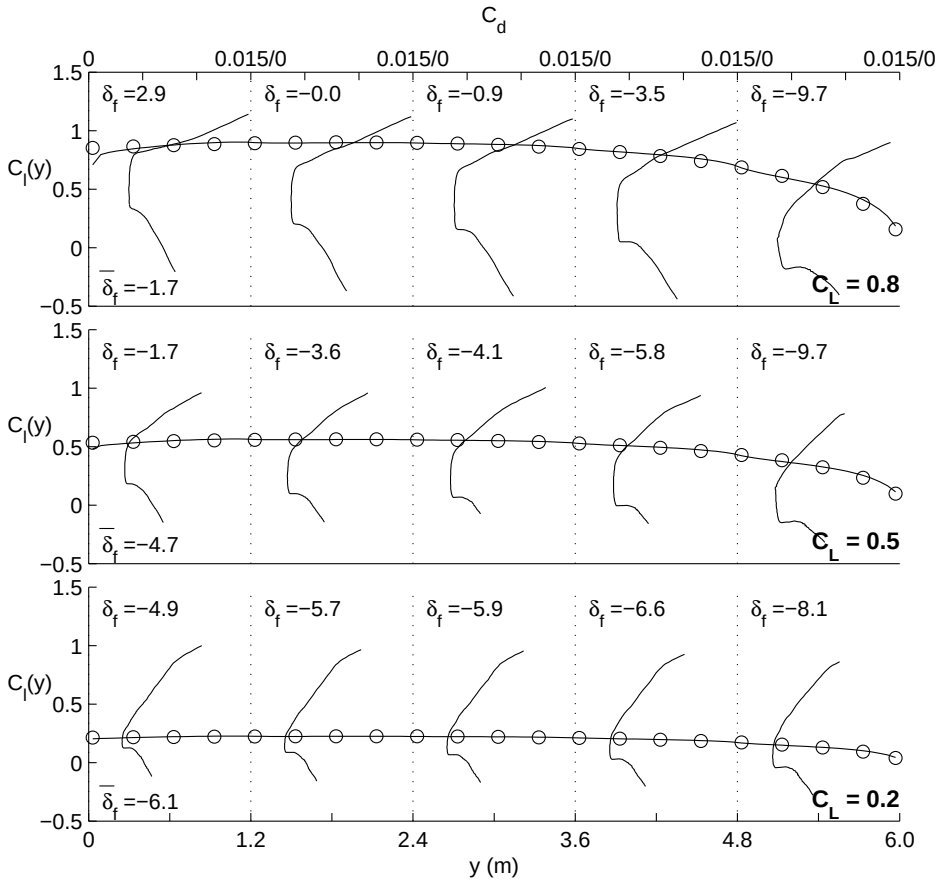

Figure 3.8: Spanwise C_l distributions with flap-section drag polars and optimal C_l distributions. Provided for C_L values of 0.2, 0.5, and 0.8 where *Scheme A* is applied.

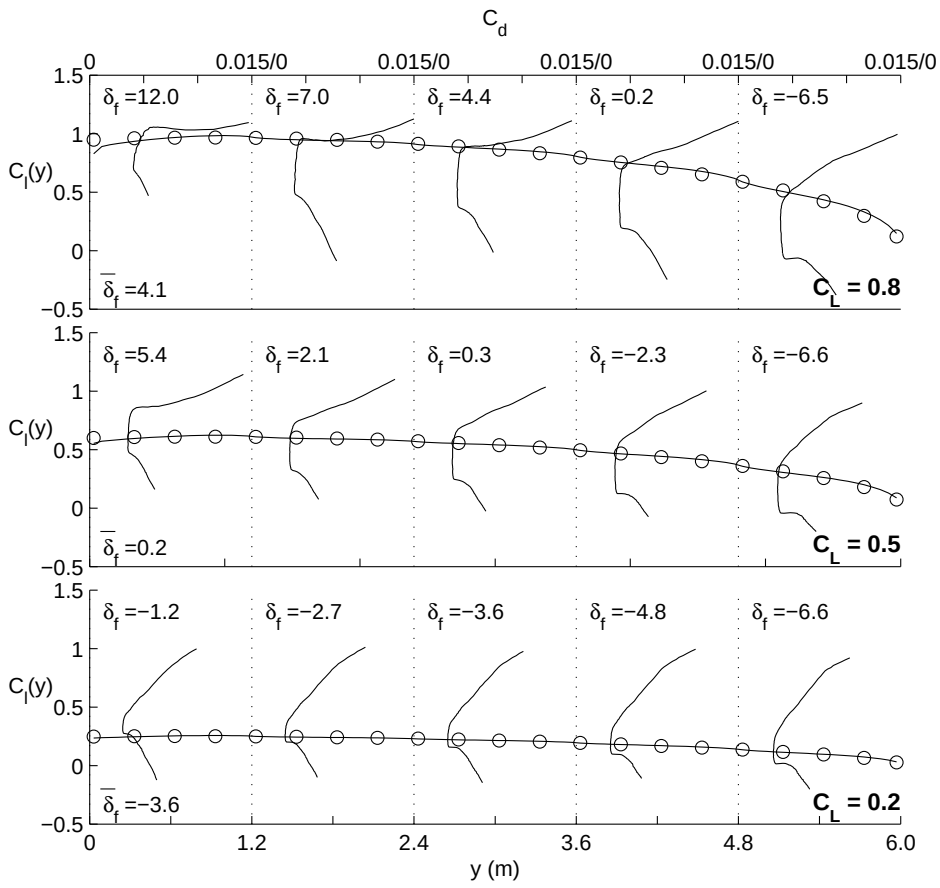

Figure 3.9: Spanwise C_l distributions with flap-section drag polars and optimal C_l distributions. Provided for C_L values of 0.2, 0.5, and 0.8 where *Scheme B* is applied.

3.1.3 Example Case #3

The third example presented returns to the sweep angle of 20 deg utilized in Sec. 3.1.1 – Example Case #1 – with the airfoil section changed to the $REFLEXED$ airfoil. Again, similar plots are displayed in Figs. 3.10 – 3.12 which present the total drag characteristics of the schemes for reducing drag.

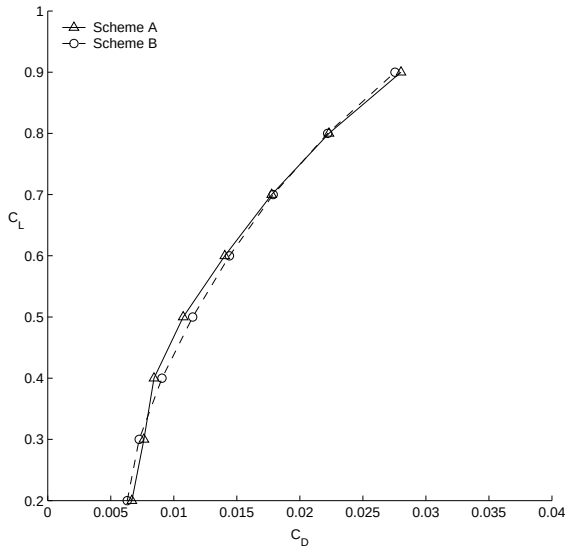

Figure 3.10: Comparison of total drag resulting from *Scheme A* and *Scheme B* for Example Case #3.

Figure 3.10 displays the total drag results, which are a bit different if compared to the results presented with the same configurations of the $CAMBERED$ airfoil. At both low and high C_L extremes, *Scheme B* tends to show optimal drag results, while at midrange C_L values it is *Scheme A* that reduces total drag. Figures 3.11 and 3.12 show the effects each scheme has on drag bucket placement. It is evident that at the low and high C_L extremes *Scheme B* will reduce profile drag, explaining why this scheme responds favorably at these conditions. However, for this configuration at midrange C_L values both schemes results in well defined low-drag-ranges, and will produce similar profile drag results. Thus, as *Scheme A* results in exactly elliptical loading, it follows that at these conditions this scheme will perform most favorably.

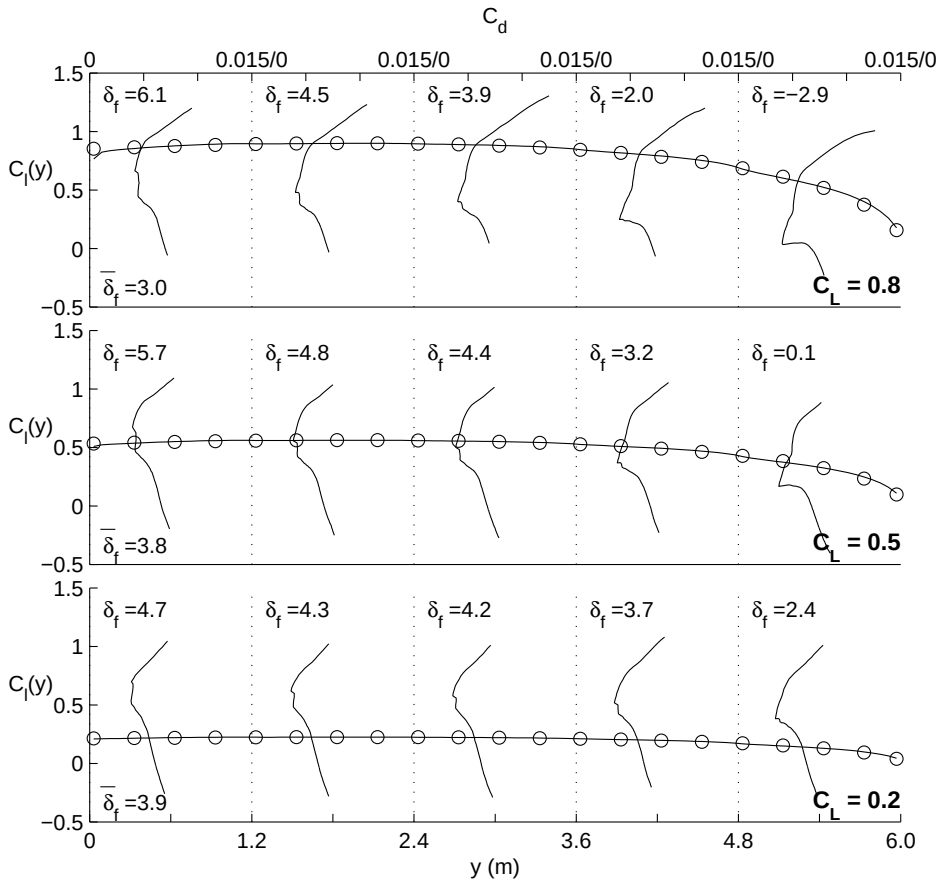

Figure 3.11: Spanwise C_l distributions with flap-section drag polars and optimal C_l distributions. Provided for C_L values of 0.2, 0.5, and 0.8 where *Scheme A* is applied.

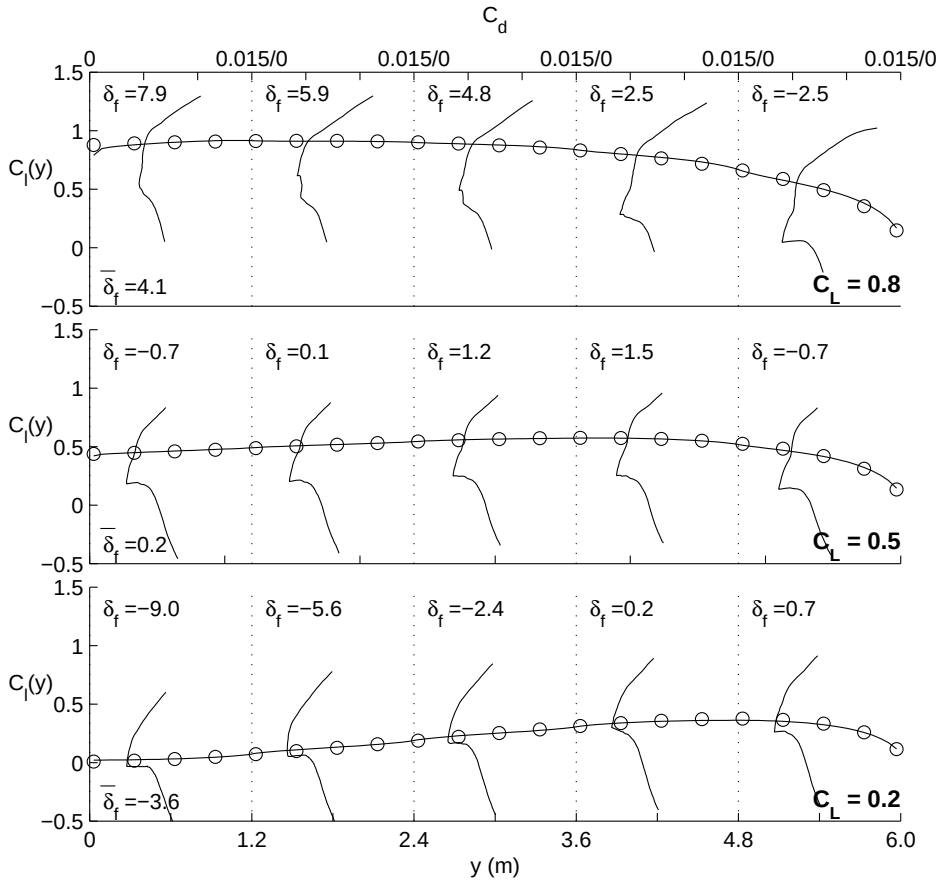

Figure 3.12: Spanwise C_l distributions with flap-section drag polars and optimal C_l distributions. Provided for C_L values of 0.2, 0.5, and 0.8 where *Scheme B* is applied.

3.1.4 Example Case #4

The final example case utilizes the same sweep angle and planform as Sec 3.1.2 – Example Case #2 – but maintains the airfoil section properties of the $REFLEXED$ airfoil used in the previous section. The total drag comparison of both drag reduction schemes is presented in Fig. 3.13, while the spanwise lift distribution plots are provided in Figs. 3.14 and 3.15.

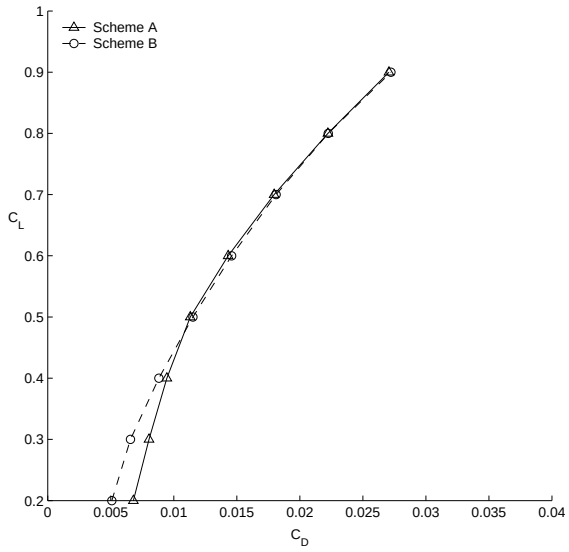

Figure 3.13: Comparison of total drag resulting from *Scheme A* and *Scheme B* for Example Case #4.

At low C_L values it is shown that the operation of the wing outside the LDR results in *Scheme A* to suffer profile drag consequences resulting in greater total drag at these conditions. This effect is similar to that found in the previous example. However, as C_L values move into the mid to high range it is evident that both schemes are operating the wing in the LDR, again resulting very similar profile drag numbers. Thus, at low C_L values *Scheme B* provides most favorable results. The two schemes converge at high C_L values, indicating that both are similarly reducing both induced and profile drag.

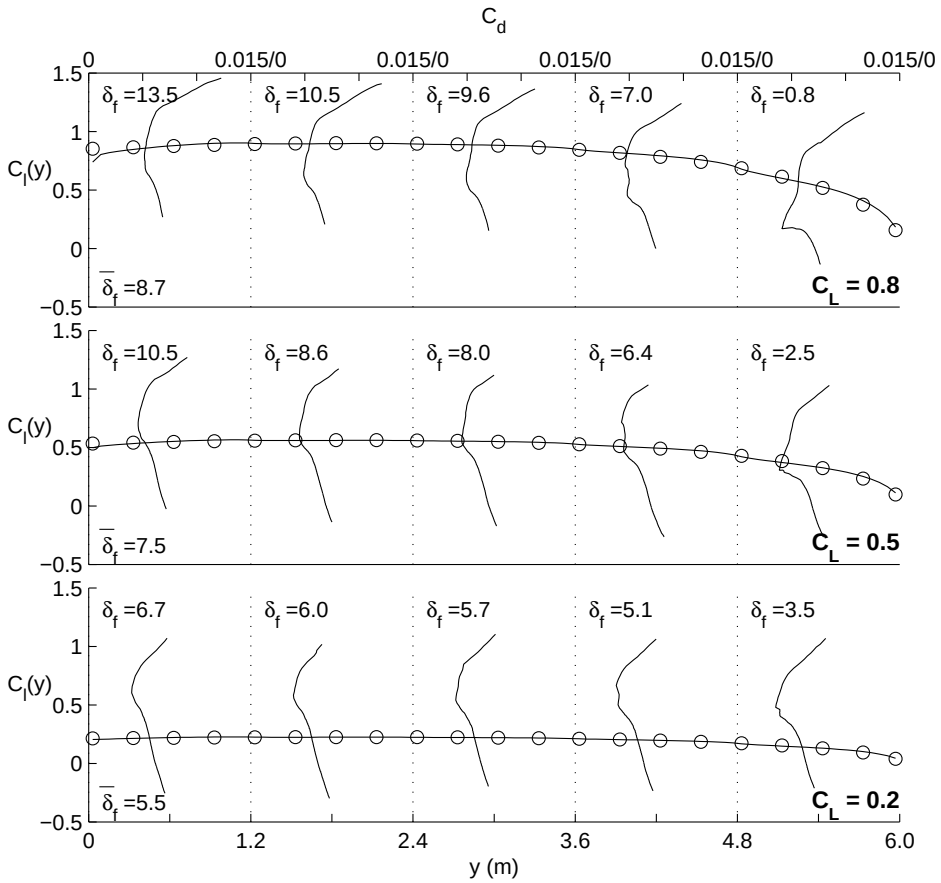

Figure 3.14: Spanwise C_l distributions with flap-section drag polars and optimal C_l distributions. Provided for C_L values of 0.2, 0.5, and 0.8 where *Scheme A* is applied.

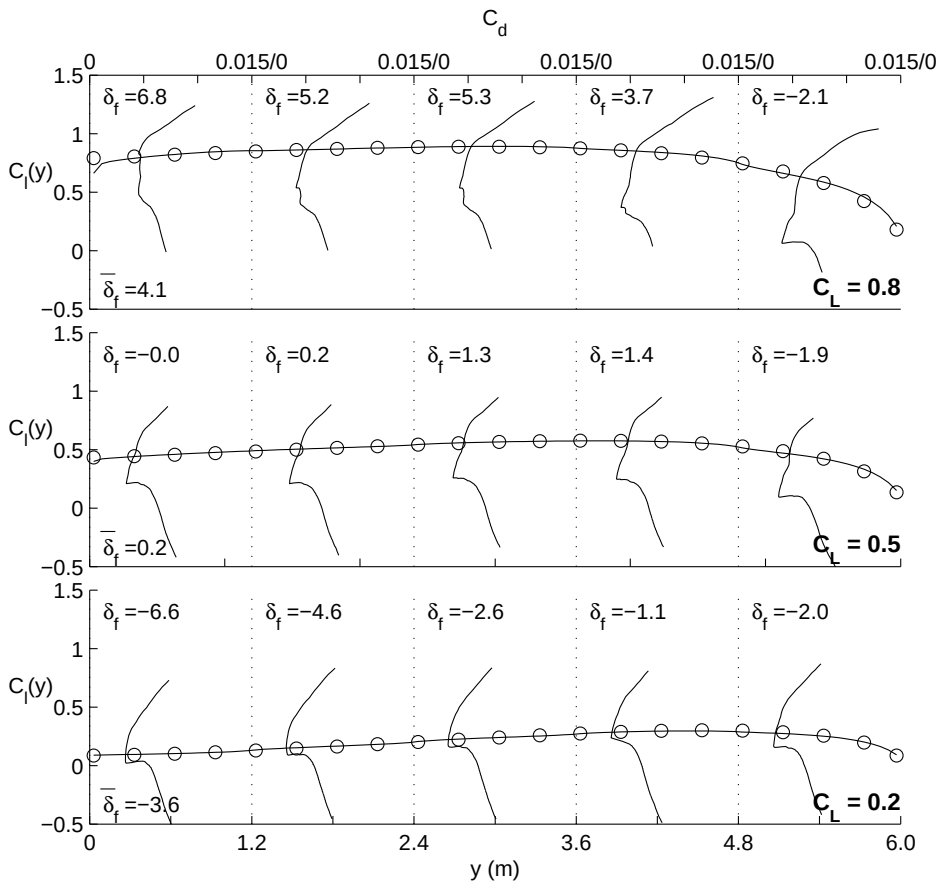

Figure 3.15: Spanwise C_l distributions with flap-section drag polars and optimal C_l distributions. Provided for C_L values of 0.2, 0.5, and 0.8 where *Scheme B* is applied.

The relationships described in the final two example cases are discussed further in Sec 3.2 and 3.3 as it can be shown that the sweep of the wing and the zero-lift pitching moment of the airfoil plays an integral part in the discussion.

3.2 Effects of Change in Sweep Angle

Highlighted in the methodology section was the importance that the governing variable $\left(C_{M_{acw}}\right)_{basic}$ has in the current problem for determining minimal induced

drag as well as achieving trim. Recall that $\left(C_{M_{ac_w}}\right)_{basic}$ describes the coefficient of the moment that is produced by the spanwise basic lift of the wing, and will be changed as the wing aerodynamic center is varied. And since the location of the wing aerodynamic center depends largely on sweep angle (Λ), it becomes necessary to study the effects that Λ has on the results obtained from the four previous example cases.

The role that $\left(C_{M_{ac_w}}\right)_{basic}$ plays for minimizing induced drag was discussed in Sec. 2.2.2. There, the constrained value of $\left(C_{M_{ac_w}}\right)_{basic}$ was solved for utilizing Eq. 2.31, and provides a good indication of the importance Λ has for determining this value. This equation is reproduced here for clarity.

$$\left(C_{M_{ac_w}}\right)_{basic}^{elliptic} = \frac{C_L}{c_{ref}} \left[Y_{ac,wing} - Y_{cp}\right] \tan(\Lambda) \tag{3.1}$$

Consider now the previous examples and compare total drag as Λ varies. Figure 3.16 displays this comparison for both *Scheme A* and *Scheme B*. Part (a) of Fig. 3.16 displays how Λ affects total drag when *Scheme A* is implemented for each airfoil. Considering Eq. 3.1, it is evident that larger values of Λ result in greater positive pitching moment produced by the basic lift. Larger Λ values are beneficial for the $CAMBERED$ airfoil as a positive static margin is desired and the section pitching moment of the airfoil is negative. This requires positive moments to offset those created by the airfoil sections, which is achieved through a combination of the basic lift and the meanflap. It follows that because when Λ is greater it creates a larger positive moment, then there is a reduced need for meanflap deflection to achieve trim. This result is displayed in Part (a) of Fig. 3.17 where the values of meanflap required to trim at each C_L is plotted for each sweep case. It is clearly seen that for the $CAMBERED$ airfoil the meanflap deflections are of substantially less magnitude for the higher sweep cases when

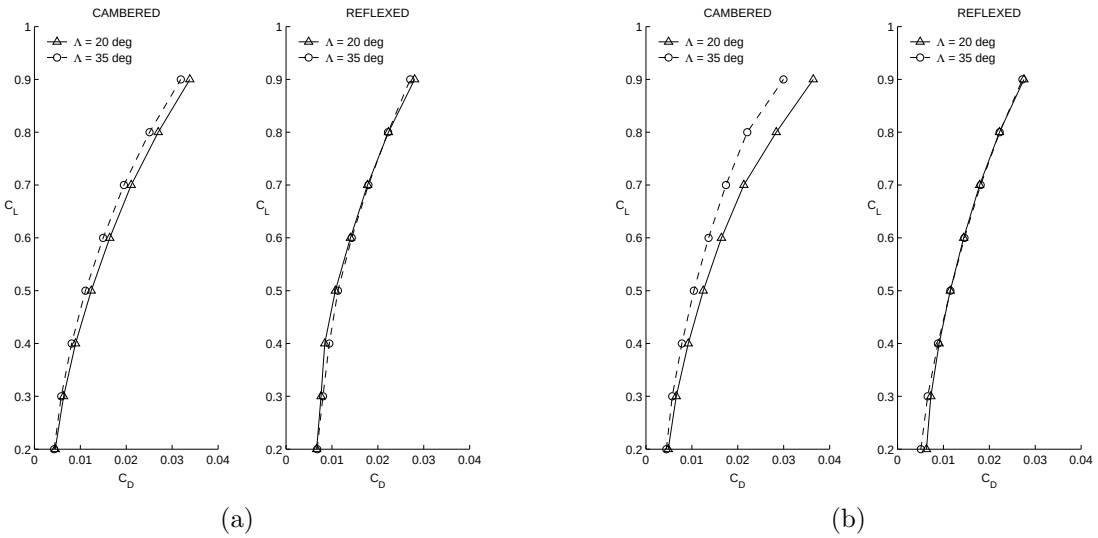

Figure 3.16: Comparison of total drag for differing sweep angles with (a) *SchemeA* applied and (b) *Scheme B* applied.

implementing *Scheme A*. And as stated previously, the lower flap deflection will result in a reduced component of profile drag and thus reduced total drag.

Considering the $REFLEXED$ airfoil in part (a) of Fig. 3.16, the effects of Λ are shown to act opposite of the $CAMBERED$ airfoil. For the $REFLEXED$ airfoil the section pitching moment is positive. Thus, as sweep increases, the pitching moment is going to grow larger, indicating a need for higher positive meanflap deflections to offset it. This is shown in part (b) of Fig. 3.17, where it follows that $\Lambda = 35$ deg will incur greater amounts of profile drag and lead to the result displayed in Fig. 3.16.

Part (b) of Fig. 3.16 displays a comparison of total drag for differing sweep angles, *SchemeB* applied. Again, it shows that higher sweep results in less total drag for the $CAMBERED$ airfoil while higher sweep will generally result in increased drag for the $REFLEXED$ airfoil. For these cases the meanflap deflections will be similar, as this is dictated by the nature of the airfoil LDR. These meanflap deflections will be small and not sufficient to trim the aircraft. Therefore, the basic lift will be necessary for counteracting the section pitching moments. In the

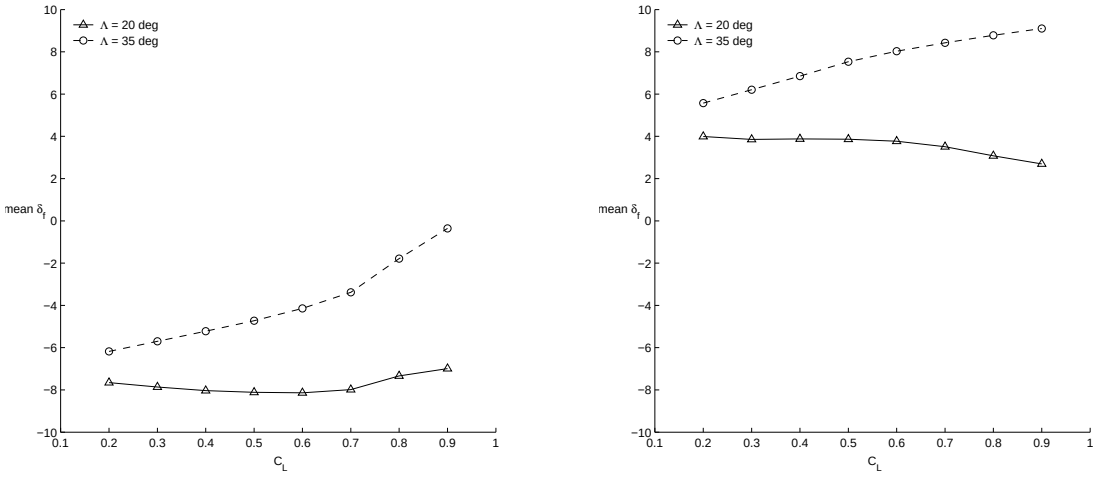

(a) (b)

Figure 3.17: Comparison of meanflap for differing sweep angles, *Scheme A* applied to (a) the $CAMBERED$ airfoil and (b) the $REFLEXED$ airfoil.

case of the $CAMBERED$ airfoil a positive moment will be required of the lift to trim, while in the case of the $REFLEXED$ airfoil a negative moment is required. It has been shown that minimum induced drag produces a positive moment and is larger at higher sweep angles, a benefit to the $CAMBERED$ airfoil, as the positive moment required will mimic the moment produced by elliptical loading. The higher sweep will again act detrimental to the $REFLEXED$ airfoil as the negative moment required by this design will create a lift distribution that pulls farther from optimal as Λ increases.

It can be deduced that for the current problem, higher sweep angles are beneficial for reducing drag. Clearly, this was shown by the $CAMBERED$ airfoil, and while the $REFLEXED$ airfoil did display the opposite effects, the drag differences were of small order. Thus, incorporating sweep should increase the design possibilities for airfoil selection and design in general of adaptive tailless aircraft utilizing these drag reduction schemes.

3.3 Effects of Change in Airfoil-Section Camber

Just as the effect that sweep has on $\left(C_{M_{ac_w}}\right)_{basic}$ was discussed in the previous section, it is important to explore how airfoil-camber change, and thus airfoil section pitching moment, has on $\left(C_{M_{ac_w}}\right)_{sections}$. The variable $\left(C_{M_{ac_w}}\right)_{sections}$ was used as a control variable to offset the moment that is produced by the spanwise lift of the wing, and is dominated by the airfoil design pitching moment as well as the wing meanflap deflection.

Figure 3.18 explores how total drag is affected when two different airfoils with similar lift and drag characteristics but substantially different zero lift pitching moment (C_{m_0}) values are utilized for the same configurations. Part (a) of the figure compares the response of the airfoils when implementing *Scheme A* for different sweep angles. Part (b) of the figure compares the response of the airfoils when implementing *Scheme B* for different sweep angles. Highlighted in the previous section was the fact that increased sweep tended to benefit the $CAMBERED$ airfoil, while increased sweep acted somewhat detrimental to the $REFLEXED$ airfoil. This fact is reinforced by Fig. 3.18, where the direct comparison of total drag shows that at lower sweep the $REFLEXED$ airfoil performs best while at higher sweep the $CAMBERED$ airfoil generally saw benefits.

When implementing *Scheme A* it is the meanflap setting that is essential for trimming the aircraft, but is also the main factor in profile drag reduction. Figure 3.19 displays the response of the meanflap when *Scheme A* is implemented. Recall that the $CAMBERED$ airfoil has a C_{m_0} of -0.0802 and the $REFLEXED$ airfoil has a C_{m_0} of 0.055. Thus, it is expected that the $CAMBERED$ airfoil will require negative meanflap settings to trim and the $REFLEXED$ airfoil will require positive settings, which is indicated by the figure. It is evident that the magnitude of meanflap deflection is lower for the $REFLEXED$ airfoil at low

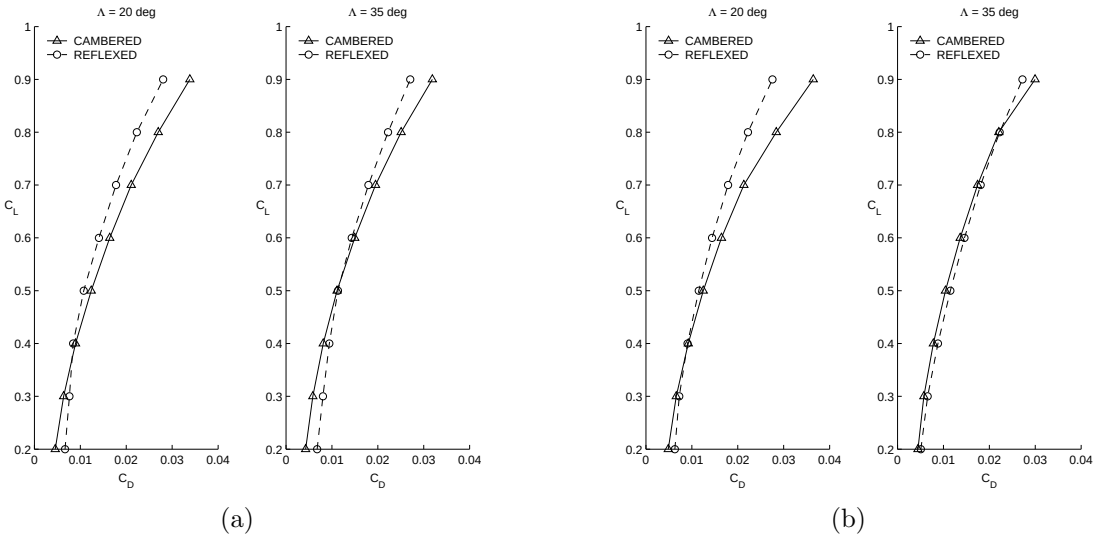

Figure 3.18: Comparison of total drag for differing airfoil camber with (a) *Scheme A* applied and (b) *Scheme B* applied.

sweep while at high sweep the magnitude of meanflap deflection is less for the $CAMBERED$ airfoil. This explains the previous section findings that has higher sweep greatly benefiting the $CAMBERED$ airfoil.

Part (b) of Fig. 3.18 represents a comparison of total drag for the cases where minimizing profile drag is the focus, and displays the influence of airfoil section pitching moment. The results presented are similar to the findings in part (a), with the $REFLEXED$ airfoil having reduced total drag at the low sweep angle, while the $CAMBERED$ airfoil performed better at increased sweep. The same arguments apply in this case as in the previous section, where the high sweep angle will bring the positive moment required to trim the $CAMBERED$ configuration nearer to elliptical loading, and thus result in lower total drag for this Λ.

The results of these comparisons display the importance that camber has on the current problem. Of particular importance is the results at the lower sweep angle. While it was highlighted in the previous section that increased sweep tends to allow greater airfoil design possibilities, this section highlights the importance that airfoil design has for reduced sweep configurations. Thus, if considering

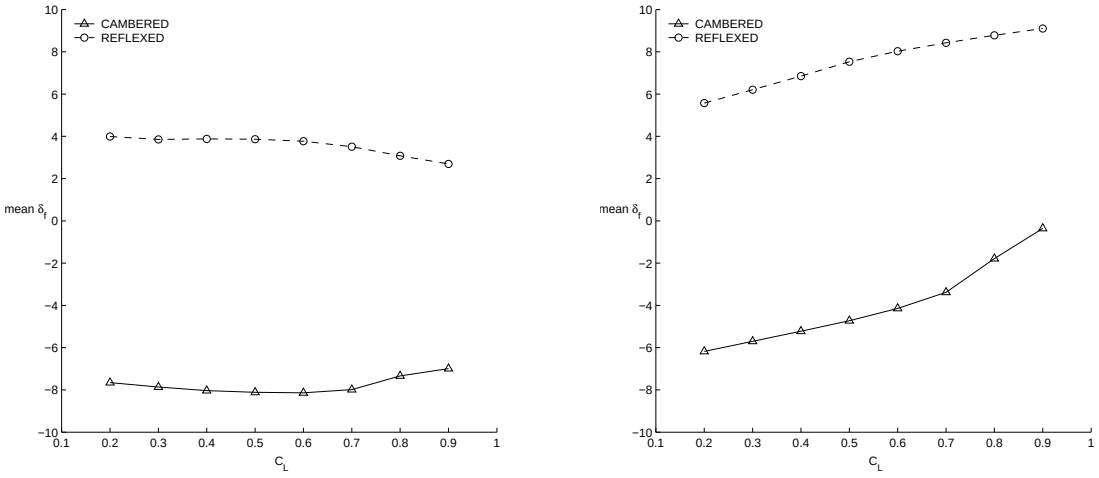

Figure 3.19: Comparison of meanflap for differing airfoil camber, *Scheme A* applied to (a) $\Lambda = 20$ deg and (b) $\Lambda = 35$ deg.

the a low-sweep design for the current methodology, utilizing a reflexed airfoil is beneficial.

3.4 Effects of Static Margin Change

Stressed throughout this thesis is the importance that longitudinal stability has for the design of tailless aircraft. In fact, it was mentioned in Sec. 1.1 that tailless aircraft have the reputation of being particularly difficult for achieving longitudinal stability and trim, and thereby limiting their usage. Thus, it was desirable to study the adaptive methods for drag reduction used by the current work with respect to differing static margins, highlighting the effects of longitudinal stability.

The previous example cases (Secs. 3.1.1 – 3.1.4) along with the sweep and camber comparisons (Secs 3.2 & 3.3) were all conducted for a hypothetical tailless aircraft which maintained a static margin of 10%. This value ensured longitudinal stability would be achieved for all tests, providing it only necessary for the methodology to achieve trim conditions. It was chosen to reduce static margin

to 0% in order to test a case of very much reduced stability, and also test static margins of 20% to test a highly stable tailless aircraft. Displayed in Figs 3.20 and 3.21 are these tests conducted for the differing schemes, airfoil sections, and sweep angles. They provide a direct comparison of how total drag is influenced margin in each case.

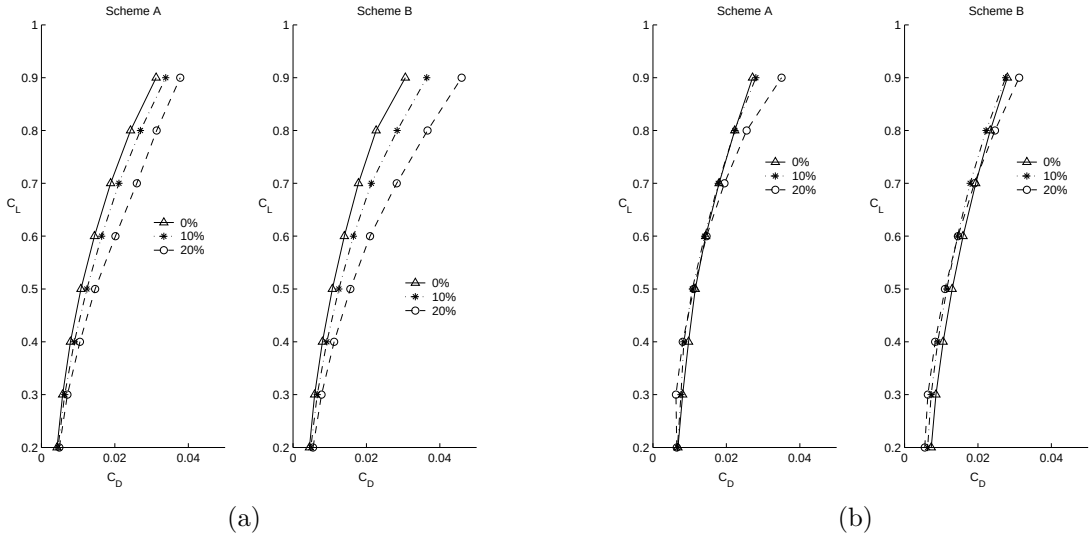

Figure 3.20: Static margin comparison for sweep angle of 20 deg for the (a) $CAMBERED$ airfoil and the (b) $REFLEXED$ airfoil.

Figure 3.20 displays total drag comparisons for the configurations where sweep angle is equal to 20 deg. It is clear in the case of the $CAMBERED$ airfoil that as static margin increases from 0% to 20%, total drag also increases, while in the case of the $REFLEXED$ airfoil, high SM does not necessary lead to high total drag. An explanation of these results is often the argument for utilizing a reflexed airfoil for tailless configurations. If one considers a trimmed aircraft with positive lift, it follows from the desirable positive SM that the pitching moment about the aerodynamic center must also be positive. And because tailless aircraft do not have a secondary horizontal surface to offset a negative moment produced by a cambered wing, it is often necessary to create a wing whose airfoil sections have a positive moment, leading directly to the reflexed airfoil section. Benefits of the

reflexed airfoil section for tailless aircraft are evident, and are displayed by this figure when compared to the cambered section.

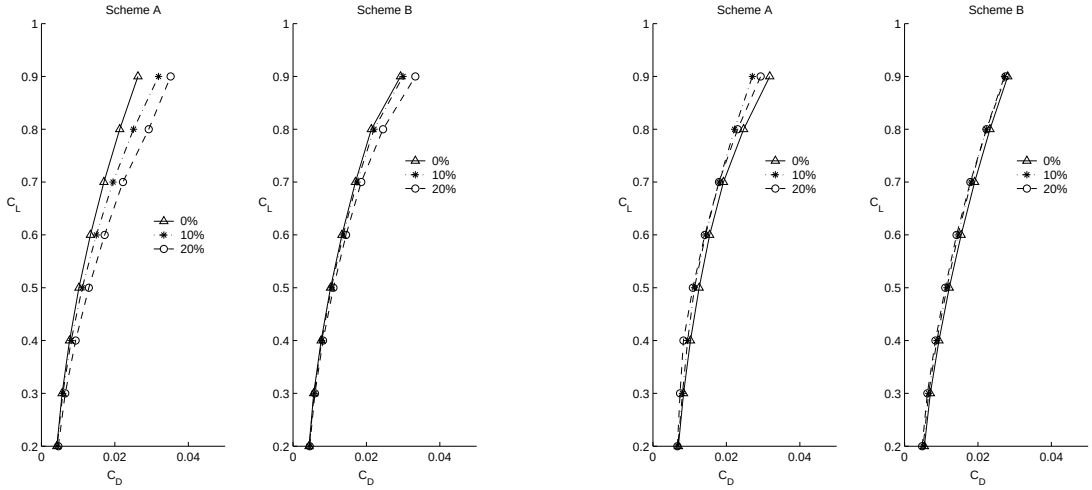

Figure 3.21: Static Margin comparison for sweep angle of 35 deg for the (a) $CAMBERED$ airfoil and the (b) $REFLEXED$ airfoil.

Figure 3.21 displays results of the same form for the 35 deg sweep cases, and indicate similar consequences of static margin change. Again, part (a) displays how the $CAMBERED$ airfoil section responds to SM change, and again it is clear that as stability is gained, drag is sacrificed. Conversely, the $REFLEXED$ airfoil section again shows benefits of increased stability, as total drag is highest when SM is 0%.

Presented in previous sections were benefits that particular design variables, namely quarter-chord sweep angle and zero-lift airfoil pitching moment, have for the the reduction of total drag. Now emphasized are the effects of another design variable, static margin, showing clearly that proper airfoil selection can result in a very stable tailless aircraft while maintaining low drag.

Chapter 4

Concluding Remarks

4.1 Summary of Results

Results have been presented pertaining to solving the problem of minimizing total drag with a longitudinal-trim constraint for an adaptive tailless aircraft. The wing adaptation method for the test cases presented here was variable spanwise camber through the use of multiple trailing-edge flaps, where the total number of 20%-chord flaps per half span was five. Methods for specific drag reduction, namely induced drag and profile drag, were tested and compared for a wide range of C_L values. The research was conducted with the intention of studying current wing adaptation techniques applied to unconventional configurations due to increased interest in the subject of wing adaptation.

Highlighted through multiple example cases are the effects that trim requirements have on reducing induced drag and profile drag for adaptive tailless aircraft. Cases were provided for tapered, planar wings with sweep angles of 20 deg and 35 deg in order to study the effects that sweep angle has on the problem. Also, each configuration was tested with both a cambered airfoil and a reflexed airfoil in order to highlight the influence of airfoil C_{m_0}.

The methodology tested proved to be successful for solving the problem at hand, as elliptical loading was achieved when induced drag was to be minimized

and the wing sections were shown to operate in the LDR when profile drag was to be minimized, with all cases maintaining longitudinal-trim and lift requirements. For each configuration total drag was presented for comparison purposes, highlighting the responses of the methodology to the different configurations. Each case provided unique results, indicating the importance of both induced and profile drag reduction. For three of the example cases, namely the $CAMBERED$ airfoil at sweep angle of 20 deg and the $REFLEXED$ airfoil at both sweep angles, it was shown that induced drag was the most important factor for reducing total drag. In the case of the $CAMBERED$ airfoil at sweep equal to 35 deg, it was shown that profile drag reduction provided optimal results.

Sweep effects were shown to be a large factor for maintaining longitudinal trim and achieving lowered drag. Highlighted were the benefits for using aft-swept configurations of 35 deg verses 20 deg for the $CAMBERED$ airfoil when implementing both induced and profile drag reduction schemes. When induced drag minimization was the primary goal, the benefits were realized due to the lesser degree of meanflap deflection necessary to trim the aircraft, while when profile drag minimization was the primary goal, it was evident that the higher sweep angle case resulted in a more elliptical load distribution, thereby reducing induced drag. For the $REFLEXED$ airfoil it was shown that lesser amounts of sweep provided greater drag benefits, however small. Thus, in considering possible design configurations for this methodology, an increased sweep angle should allow more freedom for total drag reduction.

Differences in airfoil C_{m_0} were tested through the use of two different airfoil sections: a cambered airfoil named $CAMBERED$ which maintained a C_{m_0} of -0.0802 and a reflexed airfoil named $REFLEXED$ which had a C_{m_0} of 0.055. The reflexed airfoil was designed specifically for this effort and maintained lift and drag characteristics similar to that of the cambered airfoil for comparison

purposes. Indicated by the results were the benefits for each airfoil. The positive C_{m_0} of the $REFLEXED$ airfoil proved beneficial for the drag reduction schemes at a sweep angle equal to 20 deg, while the negative C_{m_0} of the $CAMBERED$ airfoil shows benefits for the sweep cases of 35 deg. These benefits displayed by the $CAMBERED$ airfoil exist, but are small compared to the benefits shown by the $REFLEXED$ airfoil at 20 deg, thus it was shown that airfoil selection takes on greater importance at lesser sweep angles, resulting, again, in greater design possibilities for increased sweep. Along with sweep angle, the differences in C_{m_0} provided insight into how the current problem responds to design changes, and allow for direction into future design concepts.

Finally, a brief study of static margin variation was conducted, showing the tendencies of the schemes as longitudinal stability was increased and reduced. It was clear that in the case of the $CAMBERED$ airfoil, increased stability lead directly to increased drag. While in the case of the $REFLEXED$ airfoil, drag benefits were shown to increase as stability was gained. This trend further validates the use of a reflexed airfoil section for future tailless designs.

4.2 Future Work

While the study of adaptive aircraft utilizing multiple TE flaps has produced some conclusive results, this adaptation concept applied to tailless aircraft is less than mature. Opportunities exist for more comprehensive studies exploring the effects that sweep angle and airfoil camber change have on drag reduction. For instance, the limits of beneficial sweep angles could be explored relating to the effectiveness of the methodologies introduced for drag reduction with respect to longitudinal stability. This could lead to an optimal range of sweep angles for tailless aircraft employing these techniques. Also, the the results presented here point to the

possibility for specific airfoil design with respect to C_{m_0}. It has been shown that certain benefits are realized by the trend of near-zero or positive airfoil C_{m_0}, and might be furthered with more careful design.

The results presented in this thesis show beneficial trends toward a highly swept tailless aircraft, utilizing either a cambered or a reflexed airfoil. Also displayed were the benefits of utilizing a reflexed section on the lesser-swept configuration. Coincidentally, similar techniques have been employed of many of the tailless aircraft designed today, which is positive reinforcement for the ideas presented. Therefore, in the future emphasis could the placed on such designs for employing the methodology introduced by this thesis and might result in a platform for employing multiple TE flaps on a tailless aircraft for the purposes of drag reduction.

Chapter 5

References

[1] King, R. M. and Gopalarathnam, A., "Ideal Lift Distributions anf Flaps Angles for Adaptive Wings," AIAA Paper 2004–4722, August 2004.

[2] Nickel, K. and Wohlfahrt, M., *Tailless Aircraft in theory and practice*, Edward Arnold, 1994.

[3] Raymer, D. P., *Aircraft Design: A Conceptual Approach*, American Institute of Aeronautics and Astronautics, Inc., 3rd ed., 1999.

[4] Kroo, I., "Aeroelasticity of Very Light Aircraft," *Recent Trends in Aeroelasticity, Structures, and Structural Dynamics*, February 1986, pp. 187 – 202.

[5] Kroo, I., "Tailless Aircraft Design – Recent Experiences," *Symposium on Aerodynamics and Aeroacoustics*, March 1993, pp. 207 – 229.

[6] Liebeck, R. H., Page, M. A., and Rawdon, B. K., "Blended-Wing-Body Subsonic Commercial Transport," AIAA Paper 98–0438, January 1998.

[7] Bolonkin, A. and Gilyard, G. B., "Estimated Benefits of Variable-Geometry Wing Camber Control for Transport Aircraft," NASA TM 1999-206586, October 1999.

[8] Thornton, S. V., "Reduction of Structural Loads Using Maneuver Load Control on the Advanced Fighter Technology Integration (AFTI)/F-111 Mission Adaptive Wing," NASA TM 4526, September 1993.

[9] Stanewsky, E., "Aerodynamic benefits of adaptive wing technology," *Aerospace Science and Technology*, Vol. 4, 2000, pp. 439–452.

[10] Monner, H. P., Breitbach, E., Bein, T., and Hanselka, H., "Design aspects of the adaptive wing — the elastic trailing edge and the local spoiler bump," *The Aeronautical Journal*, February 2000, pp. 89–95.

[11] Spillman, J. J., "The use of variable camber to reduce drag, weight and costs of transport aircraft," *Aeronautical Journal*, 1992.

[12] McAvoy, C. W. and Gopalarathnam, A., "Automated Trailing-Edge Flap for Airfoil Drag Reduction Over a Large Lift-Coefficient Range," AIAA Paper 2002–2927, June 2002, available from http://www.mae.ncsu.edu/homepages/ashok/pubs/AIAA-2002-2927.pdf.

[13] McAvoy, C. W. and Gopalarathnam, A., "Automated Cruise Flap for Airfoil Drag Reduction Over a Large Lift Range," *Journal of Aircraft*, Vol. 39, No. 6, November–December 2002, pp. 981–988.

[14] Jones, R. T., "The Spanwise Distribution of Lift For Minimum Induced Drag of Wings Having a Given Lift and a Given Bending Moment," NACA TN 2249, December 1950.

[15] Blackwell, J. A., "Numerical Method to Calculate the Induced Drag or Optimum Loading for Arbitrary Non-Planar Aircraft," NASA SP 405, May 1976.

[16] Katz, J. and Plotkin, A., *Low-Speed Aerodynamics*, Cambridge University Press, 2001.

[17] Pfenninger, W., "Investigation on Reductions of Friction on Wings, in Particular by Means of Boundary Layer Suction," NACA TM 1181, August 1947.

[18] Pfenninger, W., "Experiments on a Laminar Suction Airfoil of 17 Per Cent Thickness," *Journal of the Aeronautical Sciences*, April 1949, pp. 227–236.

[19] Althaus, D. and Wortmann, F. X., *Stuttgarter Profilkatalog I*, Friedr. Vieweg & Sohn, Braunschweig, 1981.

[20] Somers, D. M., "Design and Experimental Results for a Flapped Natural-Laminar-Flow Airfoil for General Aviation Applications," NASA TP 1865, June 1981.

[21] Viken, J. K., *Aerodynamic Design Considerations and Theoretical Results for a High Reynolds Number Natural Laminar Airfoil*, Master's thesis, George Washington University, 1983.

[22] McGhee, R. J., Viken, J. K., Pfenninger, W., Beasley, W. D., and Harvey, W. D., "Experimental Results for a Flapped Natural-Laminar-Flow Airfoil with High Lift/Drag Ratio," NASA TM 85788, May 1984.

[23] Viken, J. K., "Boundary-Layer Stability and Airfoil Design," *Laminar Flow Aircraft Certification*, NASA CP 2413, 1985, pp. 1–30.

[24] Althaus, D., *Niedrig-geschwindigkeits-profile*, Friedr. Vieweg & Sohn Verlagsgesellschaft mbH, Braunschweig/Wiesbaden, 1996.

[25] Drela, M., "Elements of Airfoil Design Methodology," *Applied Computational Aerodynamics*, edited by P. A. Henne, Vol. 125, AIAA, Washington, DC, 1990, pp. 167–189.

[26] Kuethe, A. M. and Chow, C.-Y., *Foundations of Aerodynamics: Bases of Aerodynamic Design*, John Wiley and Sons, Inc., 5th ed., 1997.

[27] Abbott, I. H. and von Doenhoff, A. E., *Theory of Wing Sections*, Dover, New York, 1959.

[28] Selig, M. S. and Maughmer, M. D., "A Multi-Point Inverse Airfoil Design Method Based on Conformal Mapping," *AIAA Journal*, Vol. 30, No. 5, May 1992, pp. 1162–1170.

[29] Selig, M. S. and Maughmer, M. D., "Generalized Multipoint Inverse Airfoil Design," *AIAA Journal*, Vol. 30, No. 11, November 1992, pp. 2618–2625.

[30] Drela, M., "XFOIL: An Analysis and Design System for Low Reynolds Number Airfoils," *Low Reynolds Number Aerodynamics*, edited by T. J. Mueller, Vol. 54 of *Lecture Notes in Engineering*, Springer-Verlag, New York, June 1989, pp. 1–12.